

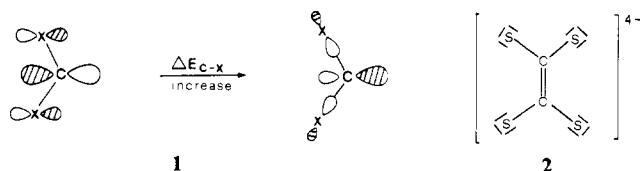
Genesis of Tetrathiooxalate-like C₂S₄ and C₂Se₄ Units. A Multiform Experimental Study and the Relevant Theoretical Implications for the Role of Transition-Metal Fragments

Claudio Bianchini,*† Carlo Mealli,*† Andrea Meli,† Michal Sabat,† and Piero Zanello†

Contribution from the Istituto per la Studio della Stereochimica ed Energetica dei Composti di Coordinazione, C.N.R., Via F. D. Guerrazzi 27, 50132 Firenze, Italy, and Dipartimento di Chimica, Università di Siena, Pian dei Mantellini, Siena, Italy. Received June 23, 1986

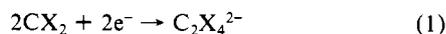
Abstract: Binuclear complexes of general formula [(triphos)M(μ-C₂X₄)M(triphos)]Y₂ [M = Rh, X = S, Se, Y = Cl⁻, BPh₄⁻, BF₄⁻, PF₆⁻; M = Ir, X = S, Y = Cl⁻, BPh₄⁻; triphos = MeC(CH₂PPh₂)₃] can be obtained from (triphos)RhCl(η²-CS₂)-C₆H₆ (**1**), (triphos)RhN₃(η²-CS₂) (**2**), (triphos)IrCl(η²-CS₂) (**3**), and (triphos)RhCl(η²-CSe₂)-C₆H₆ (**4**) after elimination of chloride or azide ligands and addition of suitable anions. The synthetic strategy favors the *head-to-head* dimerization of the dihapto-coordinated heteroallene molecules. The crystal structures of one of the precursors, **4**, and one of the products, [(triphos)Rh(μ-C₂S₄)Rh(triphos)](BPh₄)₂-CH₂Cl₂ [**10**-CH₂Cl₂ in text], have been determined by X-ray methods. Crystal data for **4** are as follows: *a* = 21.151 (6) Å, *b* = 16.450 (5) Å, *c* = 13.500 (3) Å, β = 90.81 (3)°, monoclinic, P2₁/n, Z = 4, R = 0.077. Crystal data for **10**-CH₂Cl₂ are as follows: *a* = 15.496 (4) Å, *b* = 28.736 (7) Å, *c* = 14.216 (4) Å, β = 106.02 (2)°, monoclinic, P2₁/a, Z = 4, R = 0.079. Compound **4** is a typical complex of the type L₄M(η²-CX₂) (M = d₈). The dication in **10**-CH₂Cl₂ has a dimeric framework containing a C₂S₄ bridge between two L₃M fragments. The double bond value of the C-C linkage [1.37 (3) Å] suggests the formulation of the ligand as an ethenetetrathiolate. The electrochemical behavior in nonaqueous solvents (MeCN, CH₂Cl₂) of the complexes [(triphos)Rh(μ-C₂X₄)Rh(triphos)](PF₆)₂ (X = S, Se) shows a surprisingly rich redox chemistry. The electron-transfer sequences 4+/2+, 2+/1+, 1+/0, 0/1-, and 1-/2- are thermodynamically characterizable. The compound [(triphos)Rh(μ-C₂S₄)Rh(triphos)](BF₄)₄ has been also synthesized by chemical oxidation with NOBF₄ of the 2+ derivative, whereas reduction of the latter with LiHBEt₃ yields the neutral, paramagnetic complex (triphos)Rh(μ-C₂S₄)Rh(triphos). The present family of μ-C₂X₄ complexes displays noticeable electron-transfer properties. In particular, the neutral derivative transfers electrons to 7,7,8,8-tetracyanoquinodimethane, TCNQ, to give the paramagnetic compound [(triphos)Rh(μ-C₂S₄)Rh(triphos)](TCNQ)₂, whereas [(triphos)Rh(μ-C₂S₄)Rh(triphos)](BF₄)₄ is able to extract electrons from tetrathiafulvalene to yield the 2+ derivative and the salt (TTF)₃(BF₄)₂. The electronic structure of the dimeric complexes has been investigated by using the extended Hückel method. There are two relevant π_⊥ interactions between the metals and the C₂S₄ ligand, one of which delocalizes electron density over a C₂S₄ orbital which is strongly C-C π bonding. The π_⊥ nature of three frontier MOs and their extended delocalization over the Rh(μ-C₂S₄)Rh core accounts for the rich electrochemistry of this series of compounds. The genesis of the C₂S₄ unit from two dihapto coordinated CS₂ molecules is discussed in terms of perturbation theory arguments. The relevant keystone seems to be the cleavage of the Rh-C bond in a homolytic fashion. Walsh-type diagrams show that along some possible pathways there is an *avoided crossing* between a filled metal and an empty carbon level. According to current theories on charge-transfer mechanisms, this situation could promote a *sudden electron jump* from metal to carbon. Eventually, two diradical complex species quench their paramagnetism through the formation of a σ C-C bond and through metal spin pairing within the C₂S₄ π_⊥ system.

The synthesis and X-ray characterization of the tetrathiooxalate anion is a relatively recent achievement in spite of many years of efforts from several research groups.¹ The well-known instability of C₂S₄²⁻ with respect to that of C₂O₄²⁻ is theoretically interpreted as due to the relatively smaller electronegativity difference between carbon and sulfur elements.² The shape of the CX₂ (X = O, S) FMO (fragment molecular orbital), which is used to form the C-C σ bond in C₂X₄²⁻, changes as shown in **1** for increasing ΔE_{C-X} (E = electronegativity).



Since a larger hybrid at each carbon atom is consistent with a better overlap, the argument agrees with the larger stability of the oxalate anion. Another source of instability for C₂S₄²⁻ is the direct repulsion between sulfur lone pairs. These are certainly more diffuse than the corresponding oxygen lone pairs.

Two 16-electron CX₂ molecules require at least a 2e⁻ reduction to dimerize (see eq 1). The two electrons may be provided electrochemically.³



Otherwise some transition-metal centers may favor the dimerization of carbon disulfide,⁴ although no similar metal promotion has ever been observed for carbon dioxide. Ultimately, the molecular unit C₂S₄, formed in situ, serves as a multidentate ligand toward the metal(s).

The available structural data suggest that the ligand C₂S₄, with short C-C and long C-S bonds, is better formulated as the tetra anion ethenetetrathiolate, **2**. The weakness of the C-C σ bond becomes in this case less crucial because of the cooperating C-C π bond. Moreover the engagement of the sulfur lone pairs in coordinative bonds to the metal(s) strongly attenuates their reciprocal destabilizing interactions. An ethenetetrathiolate formulation requires the transfer of four electrons from the metal(s). Why are some transition-metal fragments even more effective than electrochemistry in promoting this process?

The interaction of heteroallene molecules with transition metals has been extensively investigated over the past 10 years, and so much has been learned about their possible coordination modes and their metal-promoted reactivity. It is well-recognized that η²-C,S coordination, **3**, or η¹-C coordination, **4**, is supported by different types of transition-metal fragments whose geometrical

(1) Hoyer, E. *Comments Inorg. Chem.* **1983**, *2*, 261.

(2) Gimarc, B. M. In *Molecular Structure and Bonding*; Academic Press: New York, 1979; pp 187-192.

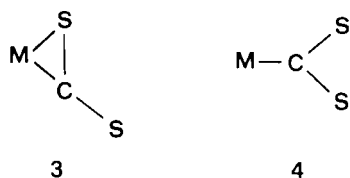
(3) Jeroschewski, P. *Z. Chem.* **1981**, *21*, 412.

(4) (a) Maj, J. J.; Rae, A. D.; Dahl, L. F. *J. Am. Chem. Soc.* **1982**, *104*, 4278. (b) Broadhurst, P. V.; Johnson, B. F.; Lewis, J.; Rathby, P. R. *J. Chem. Soc., Chem. Commun.* **1982**, 140. (c) Harris, H. A.; Rae, A. D.; Dahl, L. F. *190th National Meeting of the American Chemical Society Chicago, IL, 1985*.

* Institute C.N.R.

† University of Siena.

and electronic features can be classified.⁵



At the present moment, the organometallic chemist is very interested in finding the proper conditions to form new C–C bonds from molecules containing M–C bonds. General attention is consequently focused on the behavior of carbon monoxide, carbon disulfide, carbon diselenide, and other molecules having some characteristics of these most simple heteroallenes. It has been proposed that a C–C bond formation occurs through a free radical-like mechanism, while a two-electron reduction affords only *head-to-tail* dimerization of the group involved.⁶ Indeed, little is known about the conditions required to break homolytically the M–C bond, the step which generates the carbon free radical.

In this paper, we present a series of experimental facts on the formation, chemistry, structure and electrochemical behavior of C_2S_4 and C_2Se_4 ligands in the presence of rhodium and iridium metal fragments. The overall information serves as a support to outline theoretically an unprecedented, reasonable mechanism to the genesis of the C–C bond.

In addition to the important step relative to their formation, complexes containing $[M(\mu-C_2X_4)M]$ cores, **5**, receive a wide



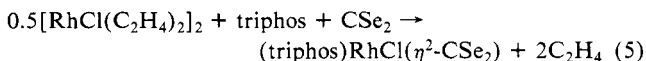
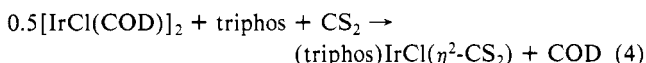
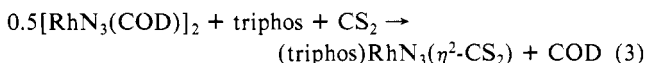
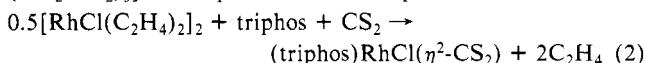
interest from other viewpoints. In fact, such cores have extensive π -electron delocalization. Accordingly, the compounds in question may exhibit an effective redox chemistry and, in some cases, present "metallic properties" such as electrical conductivity.⁷ In this respect it becomes evident the structural analogy between complexes with the framework **5** and tetrathiafulvalene, **6**, the latter being an important component of many conducting materials.⁸

A preliminary communication of part of this work has already appeared.^{9,10}

Results and Discussion

Synthesis, Characterization, and Structure of the Compounds.

Equations 2–5 describe the formation of (triphos)RhCl(η^2 -CS₂)·C₆H₆ (**1**), (triphos)RhN₃(η^2 -CS₂) (**2**), (triphos)IrCl(η^2 -CS₂) (**3**), and (triphos)RhCl(η^2 -CSe₂)·C₆H₆ (**4**), [triphos = MeC(CH₂PPh₂)₃]. The presence of a dihapto-bonded heteroallene



(5) Bianchini, C.; Mealli, C.; Meli, A.; Sabat, M. In *Stereochemistry of Organometallic and Inorganic Compounds*; Bernal, I., Ed.; Elsevier Science Publishers B. V.: Amsterdam, 1986; pp 146–254.

(6) (a) Gambarotta, S.; Fiallo, M. L.; Floriani, C.; Chiesi-Villa, A.; Guastini, C. *Inorg. Chem.* **1984**, *23*, 3532. (b) Pasquali, M.; Floriani, C.; Chiesi-Villa, A.; Guastini, C. *Inorg. Chem.* **1981**, *20*, 349.

(7) Reynolds, J. R.; Korasz, F. E.; Lillya, C. P.; Chien, J. C. W. *J. Chem. Soc., Chem. Commun.* **1985**, 268 and references therein.

(8) (a) Wudl, F. *Acc. Chem. Res.* **1984**, *17*, 227. (b) Vance, C. T.; Bereman, R. D.; Bordner, J.; Hotfield, W. E.; Helms, J. H. *Inorg. Chem.* **1985**, *24*, 2905.

(9) Bianchini, C.; Mealli, C.; Meli, A.; Sabat, M. *J. Chem. Soc., Chem. Commun.* **1984**, 1647.

(10) Bianchini, C.; Mealli, C.; Meli, A.; Sabat, M. *Inorg. Chem.* **1984**, *23*, 4125.

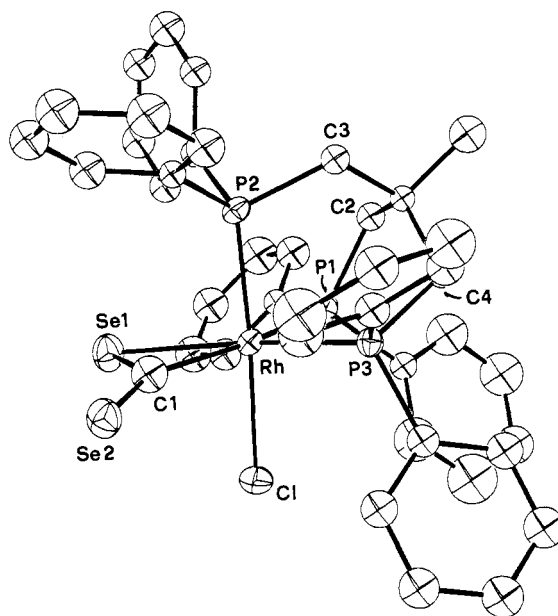


Figure 1. ORTEP drawing of (triphos)RhCl(η^2 -CSe₂). Hydrogen atoms are omitted for clarity.

Table I. Selected Bond Lengths (Å) and Angles (deg) for (triphos)RhCl(η^2 -CSe₂)·C₆H₆

Bond Lengths			
Rh–Se(1)	2.514 (4)	P(1)–C(11)	1.85 (3)
Rh–Cl	2.429 (7)	P(1)–C(12)	1.82 (2)
Rh–P(1)	2.416 (8)	P(2)–C(3)	1.85 (3)
Rh–P(2)	2.265 (7)	P(2)–C(13)	1.81 (2)
Rh–P(3)	2.339 (7)	P(2)–C(14)	1.85 (2)
Rh–C(1)	2.08 (3)	P(3)–C(4)	1.84 (3)
Se(1)–C(1)	1.90 (3)	P(3)–C(15)	1.81 (2)
Se(2)–C(1)	1.71 (3)	P(3)–C(16)	1.82 (2)
P(1)–C(2)	1.85 (3)		
Bond Angles			
Se(1)–Rh–Se(2)	85.5 (2)	Rh–P(2)–C(13)	118.4 (7)
Se(1)–Rh–P(1)	112.7 (2)	Rh–P(2)–C(14)	117.9 (6)
Se(1)–Rh–P(2)	90.7 (2)	Rh–P(3)–C(4)	109.1 (8)
Se(1)–Rh–P(3)	159.0 (2)	Rh–P(3)–C(15)	119.8 (6)
Se(1)–Rh–C(1)	47.9 (8)	Rh–P(3)–C(16)	116.4 (6)
C(1)–Rh–P(1)	92.0 (3)	C(2)–P(1)–C(11)	102 (1)
C(1)–Rh–P(2)	176.1 (3)	C(2)–P(1)–C(12)	105 (1)
C(1)–Rh–P(3)	95.1 (3)	C(1)–P(1)–C(12)	98 (1)
P(1)–Rh–P(2)	88.8 (3)	C(3)–P(2)–C(13)	104 (1)
P(1)–Rh–P(3)	88.3 (3)	C(3)–P(2)–C(14)	102 (1)
P(2)–Rh–P(3)	88.8 (3)	C(13)–P(2)–C(14)	100 (1)
P(1)–Rh–C(1)	160.4 (8)	C(4)–P(3)–C(15)	105 (1)
P(2)–Rh–C(1)	93.0 (8)	C(4)–P(3)–C(16)	106 (1)
P(3)–Rh–C(1)	111.2 (8)	C(15)–P(3)–C(16)	99 (1)
Rh–Se(1)–C(1)	53.9 (9)	Rh–C(1)–Se(1)	78 (1)
Rh–P(1)–C(2)	109.4 (8)	Rh–C(1)–Se(2)	149 (2)
Rh–P(1)–C(11)	123.2 (7)	Se(1)–C(1)–Se(2)	132 (2)
Rh–P(1)–C(12)	117.1 (6)		
Rh–P(2)–C(3)	111.7 (8)		

molecule in compounds **1–4** is inferred by means of IR spectroscopy. The M– η^2 -CS₂ moiety exhibits two typical vibrations, namely the out-of-ring $\nu(\text{C}=\text{S})$ in the region 1160–1110 cm⁻¹ and the in-ring $\nu(\text{C}=\text{S})$ in the region 650–600 cm⁻¹,⁵ whereas the M– η^2 -CSe₂ moiety shows a $\nu(\text{C}=\text{Se})$ stretching vibration in the region 1000–950 cm⁻¹.¹¹ Accordingly, the IR spectra of **1–4** contain absorptions at 1160;640, 1150;630, 1140;650, and 970 cm⁻¹, respectively. A strong absorption at 2020 cm⁻¹ in the IR spectrum of **2** is due to the terminal N₃⁻ ligand.

The crystal structure of **4** has been determined by X-ray methods. An ORTEP drawing of the molecule is shown in Figure 1. Selected bond distances and angles are reported in Table I.

(11) Werner, H.; Ebner, M. *J. Organomet. Chem.* **1983**, *258*, C52.

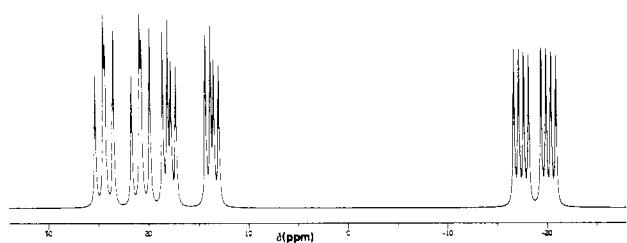
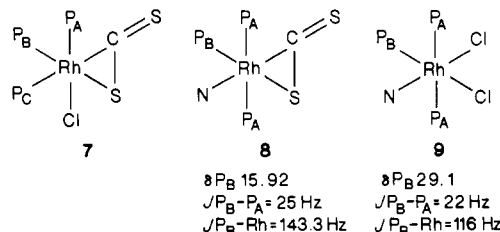


Figure 2. Calculated ³¹P{¹H} NMR spectrum of (triphos)RhCl(η²-CS₂).

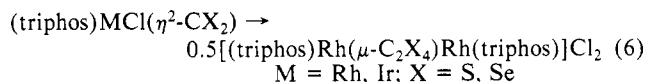
The structure is typical of a heteroallene molecule dihapto bonded to a transition-metal fragment of type L₄M with pseudo C_{2v} symmetry. The phosphorus atoms of triphos occupy three fac positions of an octahedron, the three P-Rh-P angles being only a bit less than 90°, as usual. The coordination of the supporting metal fragment is completed by a chloride ligand trans to the P(2) atom. The CSe₂ molecule is practically coplanar with the P(1)-Rh-P(3) moiety (dihedral angle between the two planes 6.3°). Important structural aspects of **4** have been already commented on.⁹ In particular, the large bending of CSe₂ [Se-C-Se angle = 132 (2)°] and the long η²-coordinated C-Se linkage [compare its value of 1.90 (3) Å with the value found in the complex [1,2-C₆H₄(CH₂PPh₂)₂]Pd(η²-SeCS), 1.80 (2) Å]¹² are indicative of large π_⊥ back-donation from the metal. All of the Rh-P bonds are different, the shortest being the one trans to the chlorine atom. Interestingly, the Rh-P bond trans to the carbon atom is much longer than the other equatorial Rh-P bond trans to the selenium atom [2.416 (8) vs. 2.339 (7) Å]. A similar feature was observed in L₂M(η²-CS₂) complexes [M = Pd, Pt; L = PPh₃].¹³ Moreover in the very comparable rhodium(I) complex [(np₃)Rh(η²-CS₂)]BPh₄ (**5**)¹⁴ [np₃ = N(CH₂CH₂PPh₂)₃], the carbon atom is trans to the nitrogen atom which, with rhodium and one phosphorus atom, defines the equatorial plane. The Rh-N bond of 2.30 (1) Å is almost as long as the Rh-P bond [2.345 (5) Å] trans to the coordinated sulfur atom. All this is indicative that in η²-coordination the preferential orientation of the heteroallene is such that the least σ electron density is located trans to the carbon atom. In fact, either the weaker amine ligand sits in this position, or a much longer distance is observed when two equally strong donors act as equatorial ligands. Notice that in complexes **4** and **5**, the Rh-C distance is practically the same [2.08 (3) and 2.08 (2) Å, respectively]. However, when the equatorial ligands are strong π acceptors, such as CO, the above trend seems modified by the formation of π bonds. In the complex (PPh₃)(PMe₃)(CO)₂Fe(η²-CS₂),¹⁵ the Rh-C bond trans to the carbon atom is the shortest [1.77 vs. 1.80 Å].

The primary geometry of **4** can be extended to **1**, **2**, and **3**. The ³¹P{¹H} NMR spectra of **1**, **2**, and **4** consist of very similar ABCX patterns, whereas that of **3** exhibits an ABC pattern. As an example, we report in Figure 2 the calculated spectrum of **1**, which is identical with the observed spectrum in CD₂Cl₂ at 213 K. The ³¹P NMR assignments are as follows: δ P_A 22.55 (J_{P_A-P_B} = 26.7 Hz, J_{P_A-P_C} = 32.4 Hz, J_{P_A-Rh} = 117.2 Hz), δ P_B 15.78 (J_{P_B-P_C} = 15.9 Hz, J_{P_B-Rh} = 137.4 Hz), δ P_C -18.75 (J_{P_C-Rh} = 88.7 Hz). The assignments for **1** (sketch **7**) have been made by reference to existing ³¹P NMR data, and, in particular, to the data for the complex **5**¹⁴ and [(np₃)RhCl₂]BPh₄ (**6**)¹⁶ (sketches **8** and **9**, respectively). In fact, on the basis of both the chemical shifts and coupling constants, the resonances at 22.55 and 15.78 ppm in the spectrum of **1** may be assigned to P_A and P_B, respectively. The highfield resonance of P_C suggests that the ligand trans to the

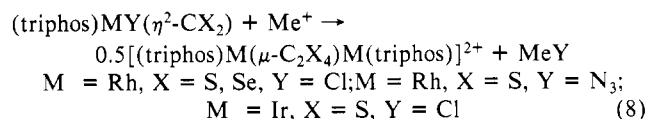
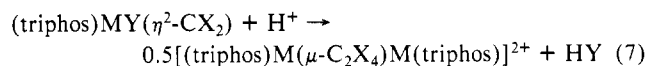


carbon atom has a different nature, as already envisaged by the structural analysis.

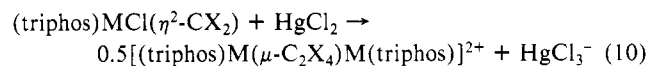
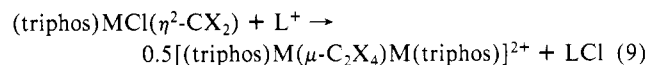
Compounds **1-4** are stable in the solid state and in deoxygenated CH₂Cl₂ solutions in which they behave as nonelectrolytes. The addition of alcohols (EtOH, MeOH, 1-butanol) to CH₂Cl₂ solutions of **1**, **3**, and **4** causes a rapid chromatic change and a marked increase in conductivity. On slow evaporation of the solvent, [(triphos)Rh(μ-C₂S₄)Rh(triphos)]Cl₂ (**7**), [(triphos)Ir(μ-C₂S₄)Ir(triphos)]Cl₂ (**8**), and [(triphos)Rh(μ-C₂Se₄)Rh(triphos)]Cl₂ (**9**), are formed in quantitative yields (eq 6).



Methatetical reactions with NaBPh₄ give the corresponding bis(tetraphenylborate) complexes [(triphos)M(η²-C₂X₄)M(triphos)](BPh₄)₂ [M = Rh, X = S (**10**); M = Ir, X = S (**11**); M = Rh, X = Se (**12**)]. At variance with the behavior of **1**, **3**, and **4**, compound **2** is stable in CH₂Cl₂/alcohol solutions. However, like **1**, **3**, and **4**, it is rapidly converted to **10** by reaction with HOSO₂CF₃, HBF₄, or MeOSO₂CF₃, followed by NaBPh₄ addition (eq 7, 8).

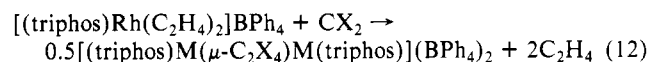
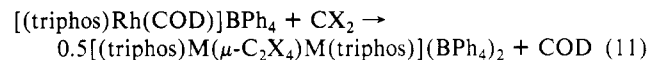


12, respectively but not that of **2** to **10** are promoted also by other Lewis acids such as Ag⁺, Tl⁺, alkali cations (L), or HgCl₂ (eq 9, 10).



It is noteworthy that **1**, **3**, and **4** are stable in CH₂Cl₂ solution or in THF suspension in the presence of (NBu₄)BPh₄ or (PPN)BPh₄, but rapidly degrade to the corresponding μ-C₂X₄ dimers when treated with NaBPh₄.

Finally, **10** and **12** are quantitatively formed by reacting [(triphos)Rh(COD)]BPh₄¹⁷ or [(triphos)Rh(C₂H₄)₂]BPh₄¹⁷ with CS₂ or CSe₂ (eq 11, 12).



The crystal structure of **10**·CH₂Cl₂ has been established by means of an X-ray analysis. An ORTEP drawing is reported in Figure 3. Selected bond distances and angles are reported in Table II.

The complex cation consists of two (triphos)Rh units bridged by a C₂S₄ ligand. The dimer is centrosymmetric, and the relative orientation of the bridge with respect to each terminal L₃M fragment is such that each metal is approximately square py-

(12) Werner, H.; Ebner, M.; Bertleff, W.; Schubert, U. *Organometallics* **1983**, *2*, 891.

(13) (a) Mason, R.; Rae, A. I. M. *J. Chem. Soc. A* **1970**, 1767. (b) Kashiwagi, T.; Yasuoka, N.; Ueki, T.; Kasai, M.; Kokudo, M.; Takahashi, S.; Hagihara, N. *Bull. Chem. Soc. Jpn.* **1968**, *41*, 296.

(14) Bianchini, C.; Masi, D.; Mealli, C.; Meli, A.; Sabat, M. *Organometallics* **1985**, *4*, 1014.

(15) Le Bozec, H.; Dixneuf, P. H.; Carty, A. J.; Taylor, N. J. *Inorg. Chem.* **1978**, *17*, 2568.

(16) Di Vaira, M.; Peruzzini, M.; Zanobini, F.; Stoppioni, P. *Inorg. Chim. Acta* **1983**, *69*, 37.

(17) The synthesis and characterization of these two compounds are the subject of a manuscript in preparation.

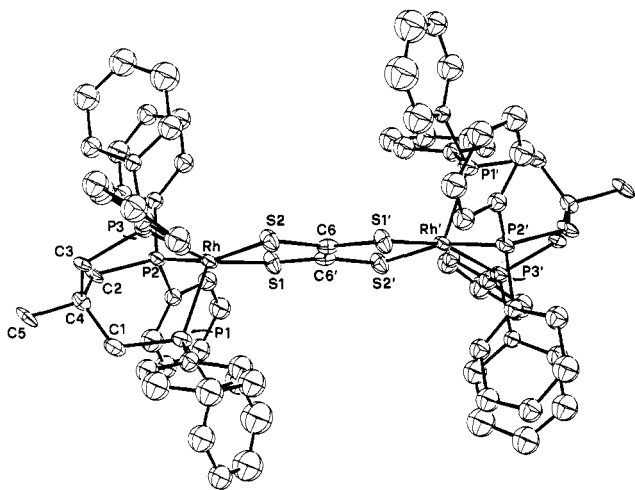


Figure 3. ORTEP drawing of the $[(\text{triphos})\text{Rh}(\mu\text{-C}_2\text{S}_4)\text{Rh}(\text{triphos})]^{2+}$ complex cation. Hydrogen atoms are omitted for clarity.

Table II. Selected Bond Lengths (Å) and Angles (deg) for $[(\text{triphos})\text{Rh}(\mu\text{-C}_2\text{S}_4)\text{Rh}(\text{triphos})](\text{BPh}_4)_2\cdot\text{CH}_2\text{Cl}_2$

Bond Lengths			
Rh-P(1)	2.244 (5)	C(6)-C(6)	1.37 (3)
Rh-P(2)	2.307 (5)	C(1)-P(1)	1.83 (2)
Rh-P(3)	2.334 (6)	C(2)-P(2)	1.83 (2)
Rh-S(1)	2.311 (6)	C(3)-P(3)	1.82 (2)
Rh-S(2)	2.296 (5)	C(5)-C(4)	1.55 (2)
C(6)-S(1)	1.76 (2)	C(4)-C(3)	1.52 (2)
C(6)-S(2)	1.70 (2)	C(4)-C(2)	1.55 (2)
		C(4)-C(1)	1.52 (2)
Bond Angles			
S(1)-Rh-S(2)	85.9 (2)	S(2)-Rh-P(2)	159.2 (2)
S(1)-Rh-P(1)	107.4 (2)	S(2)-Rh-P(3)	87.1 (2)
S(1)-Rh-P(2)	91.9 (2)	S(1)-C(6)-S(2)	118.3 (2)
S(1)-Rh-P(3)	163.2 (2)	S(1)-C(6)-C(6)	116.8 (2)
P(1)-Rh-P(2)	88.6 (2)	C(6)-S(2)-Rh	105.1 (6)
P(1)-Rh-P(3)	89.4 (2)	C(1)-P(1)-Rh	112.3 (6)
P(2)-Rh-P(3)	89.2 (2)	C(2)-P(2)-Rh	112.9 (6)
S(2)-Rh-P(1)	111.8 (2)	C(3)-P(3)-Rh	112.8 (6)

ramidal. The apical vector Rh-P(1) is the shortest among the Rh-P bonds [2.244 (5) Å]. The C₂S₄ unit is planar by symmetry, but the Rh(μ-C₂S₄)Rh core is not, each rhodium atom being ca. 0.3 Å from the C₂S₄ plane. The short C-C bond of 1.37 (3) Å is equal to that found [1.36 (1) Å] in $[(\text{C}_5\text{Me}_5)\text{Ni}(\mu\text{-C}_2\text{S}_4)\text{Ni}(\text{C}_5\text{Me}_5)]$,^{4a} the other known binuclear species containing the C₂S₄ ligand. However, the C-C bond is slightly shorter in the tetranuclear compound $[(\text{CO})_6\text{Fe}_2(\mu\text{-C}_2\text{S}_4)\text{Fe}_2(\text{CO})_6]$,^{4b} i.e., 1.33 (1) Å. The C-C bond is longer [1.390 (15) Å] in the mononuclear complex $(\text{PPh}_3)(\text{CO})_2\text{Fe}[\text{S}_2\text{C}_2(\text{SMe})_2]$,¹⁸ where the C₂S₄ unit acts as a 1,2-dithiolene chelate ligand toward only one metal while the other two methylated sulfur atoms lie in terminal positions. Finally, the C-C bond is 1.461 (19) Å in the free tetrathiooxalate dianion.¹⁹ A comparison between all the structures containing the C₂S₄ unit also shows that the shorter are the C-C bonds, the longer are the C-S ones. In fact, the average C-S distance is as long as 1.77 Å in the tetranuclear iron compound (close to the C-S single bond) but is only 1.70 (1) Å in the mononuclear complex of the same metal and in the uncoordinated species. In **10** the C-S bonds average 1.73 (2) Å. These structural details of the C₂S₄ ligand are useful for the understanding of the relative electronic distribution (see one of the next sections of the paper).

The ³¹P{¹H} NMR spectrum (CD₂Cl₂, 293 K) of **10** consists of a single resonance at 30.59 ppm (*J*_{P-Rh} = 106.3 Hz). This pattern does not vary with the temperature (303–213 K) and is

(18) Touchard, D.; Fillaut, J.-L.; Dixneuf, P.; Mealli, C.; Sabat, M.; Toupet, L. *Organometallics* **1985**, *4*, 1684.

(19) Lurd, H.; Hoyer, E.; Gronbaek Haell, R. *Acta Chem. Scand. B* **1982**, *36*, 207.

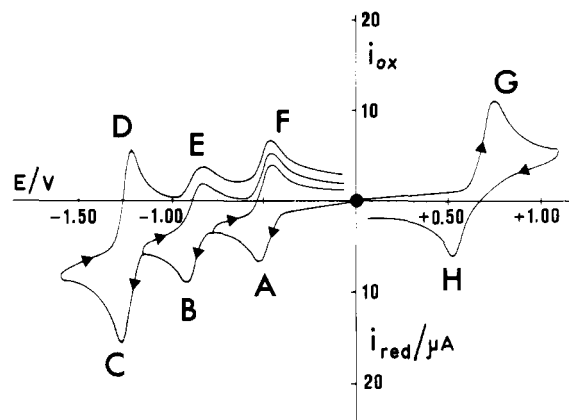
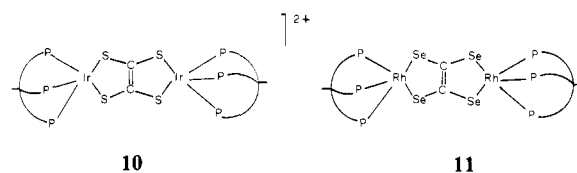
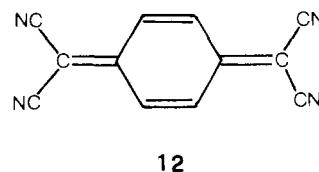


Figure 4. Cyclic voltammetric response recorded on a MeCN solution containing $[(\text{triphos})\text{Rh}(\mu\text{-C}_2\text{S}_4)\text{Rh}(\text{triphos})](\text{PF}_6)_2$ (4.0×10^{-4} mol dm⁻³) and $(\text{NEt}_4)\text{ClO}_4$ (0.1 mol dm⁻³). Platinum working electrode. Scan rate 0.2 V s⁻¹; (●) starting potential.

consistent with the rapid intramolecular exchange of the three phosphorus atoms of triphos around the rhodium atoms.¹⁴ Compounds **11** and **12** display identical ³¹P NMR patterns with



single resonances at 3.27 (CDCl₃, 293 K) and 31.00 ppm (CD₂Cl₂, 293 K, *J*_{P-Rh} = 105.2 Hz), respectively. The IR spectra of the 1:2 electrolytes **10**, **11**, and **12** (see Experimental Section) contain



no $\nu(\text{C}=\text{S})$ or $\nu(\text{C}=\text{Se})$. On the basis of all of these data it is reasonable to assign to **11** and **12** the complex framework found for **10**. Accordingly, an ethenetetrathiolate ligand bridges two (triphos)Ir fragments in **11** (sketch **10**), whereas an ethene-tetraselenolate ligand bridges two (triphos)Rh fragments in **12** (sketch **11**).

Electrochemistry. The cyclic voltammetric behavior of $[(\text{triphos})\text{Rh}(\mu\text{-C}_2\text{S}_4)\text{Rh}(\text{triphos})](\text{PF}_6)_2$ (**13**) in MeCN solution is shown in Figure 4. One anodic and three cathodic processes are observed. Controlled potential coulometric tests were carried out at a mercury pool or at a platinum gauze macroelectrode for the reduction processes and at a platinum gauze for the oxidation process. The cathodic processes occurring at peaks A and B involve a one-electron charge transfer, whereas the third cathodic process (peak C) involves a two-electron charge transfer. The anodic process occurring at peak G involves a two-electron charge transfer. As for the cathodic process occurring at the peak system A/F, the analysis of cyclic voltammetric responses with scan rates varying from 0.02 to 50 V s⁻¹ shows the following features: the value of the $i_{\text{p(F)}}/i_{\text{p(A)}}$ ratio is constantly equal to 1; the $i_{\text{p(A)}}v^{-1/2}$ term is constant; the $(E_{\text{p(F)}} - E_{\text{p(A)}})$ value is constantly equal to 60 mV except for scan rates higher than 2 V s⁻¹ where it gradually increases up to 80 mV at 50 V s⁻¹ likely on account of an uncompensated solution resistance. All of these data are diagnostic of a one-electron reversible charge transfer²⁰ leading to the stable species $[(\text{triphos})\text{Rh}(\mu\text{-C}_2\text{S}_4)\text{Rh}(\text{triphos})]^+$. A formal electrode potential of -0.49 V can be computed as the average value between $E_{\text{p(A)}}$ and $E_{\text{p(F)}}$ for the redox couple $[(\text{triphos})\text{Rh}(\mu\text{-C}_2\text{S}_4)\text{Rh}$

(20) Brown, E. R.; Large, R. F. In *Physical Methods of Chemistry*; Weissberger, A., Rossiter, B. W., Eds.; Wiley: New York, 1971; Part 11A.

(triphos)] $^{2+}$ /[(triphos)Rh(μ - C_2S_4)Rh(triphos)] $^{+}$. Cyclic voltammograms for the cathodic process occurring at the peak system B/E, reveal that, at least at low scan rates, the value of the $i_{p(E)}/i_{p(B)}$ ratio is less than 1 (e.g., 0.90 at 0.02 V s^{-1}). The value of $(E_{p(E)} - E_{p(B)})$ increases from 70 to 94 mV on going from scan rate 0.02 V s^{-1} to scan rate 0.5 V s^{-1} , while the $i_{p(E)}v^{-1/2}$ term is constant. These data together with the coulometric ones, are indicative of a one-electron quasireversible charge transfer complicated by a slow chemical reaction. Although there are some graphical difficulties to fix the conditions where the $i_{p(E)}/i_{p(B)}$ ratio becomes unitary, a formal electrode potential of -0.87 V can be attributed to the redox couple [(triphos)Rh(μ - C_2S_4)Rh(triphos)] $^{+}$ /[(triphos)Rh(μ - C_2S_4)Rh(triphos)] 0 .

The analysis of the cyclic voltammograms for the peak system C/D shows that at scan rate 0.02 V s^{-1} , the ratio $i_{p(D)}/i_{p(C)}$ is 0.88; the $(E_{p(D)} - E_{p(C)})$ difference gradually increases from 46 to 58 mV when the scan rate increases from 0.02 to 0.5 V s^{-1} . The $i_{p(C)}v^{-1/2}$ term is constant and about twice the corresponding parameter for the other two cathodic processes. These data are indicative of a quasireversible two-electron charge transfer complicated by a slow chemical reaction, in which two electrons are sequentially added at the same electrode potential of -1.24 V . Controlled potential electrolyses confirm this interpretation. In the case of the first reduction process, after the consumption of 1 mol of electrons per mol of the starting compound at $E_w = -0.7 \text{ V}$, the cyclic voltammogram picture is wholly consistent with the electrogeneration of [(triphos)Rh(μ - C_2S_4)Rh(triphos)] $^{+}$. This specimen is stable over the relatively long time of the electrolytic experiment. In the case of the other cathodic processes, cyclic voltammograms, after the relevant exhaustive electrolysis, show a decomposition of the initial molecular framework.

The two-electron anodic process occurring at the peak system G/H was examined both by cyclic voltammetry at different scan rates and by chronoamperometry in the time range 0.002–3 s. The analysis seems to indicate that, in the time scale of these techniques, the oxidation process involves an uncomplicated quasireversible two-electron charge transfer at the potential of $+0.64 \text{ V}$. However, as it will be discussed in the following two sections, the two-electron charge transfer which leads to the formation of the oxidized species [(triphos)Rh(μ - C_2S_4)Rh(triphos)] $^{4+}$ is likely accompanied by an overall conformational rearrangement of the dimeric framework. In addition, the C_2S_4 unit undergoes the rearrangement from ethenetetrathiolate to tetrathiooxalate group. In this respect, it is noteworthy that structural changes concomitant with charge transfers have been recently pointed out and discussed.²¹ Hence, it is reasonable to deduce that the quasireversibility of the $2+/4+$ process is attributable to the innersphere reorganization energy which, by contributing to the activation barrier of the electron-transfer, slows down the rate of the charge transfer.

The electrochemical investigation points out the possibility of electrogenerating both the monocation [(triphos)Rh(μ - C_2S_4)Rh(triphos)] $^{+}$ and the tetracation [(triphos)Rh(μ - C_2S_4)Rh(triphos)] $^{4+}$. In this regard, Figure 5 shows the cyclic voltammograms recorded on solutions of [(triphos)Rh(μ - C_2S_4)Rh(triphos)] $^{2+}$ after exhaustive electrolysis both at the two-electron oxidation process (Figure 5a) and at the first one-electron reduction process (Figure 5b). It is clearly evident that both the tetracation and the monocation are stable species and that their electrogeneration does not lead to irreversible structural changes of the primitive molecular structure.

Also, notice that the unusual ability of [(triphos)Rh(μ - C_2S_4)Rh(triphos)] $^{2+}$ to undergo many sequential, thermodynamically characterizable, electron-transfer sequences ($4+/2+$, $2+/1+$, $1+/0$, $0/2-$) can be attributed to its intrinsic electronic configuration. In fact, we have tested the electrochemical behavior of both (triphos)RhCl(η^2 -CS $_2$) and triphos itself. The former compound, which can be formally considered the precursor of the dimer, gives rise in MeCN solution to irreversible oxidation and

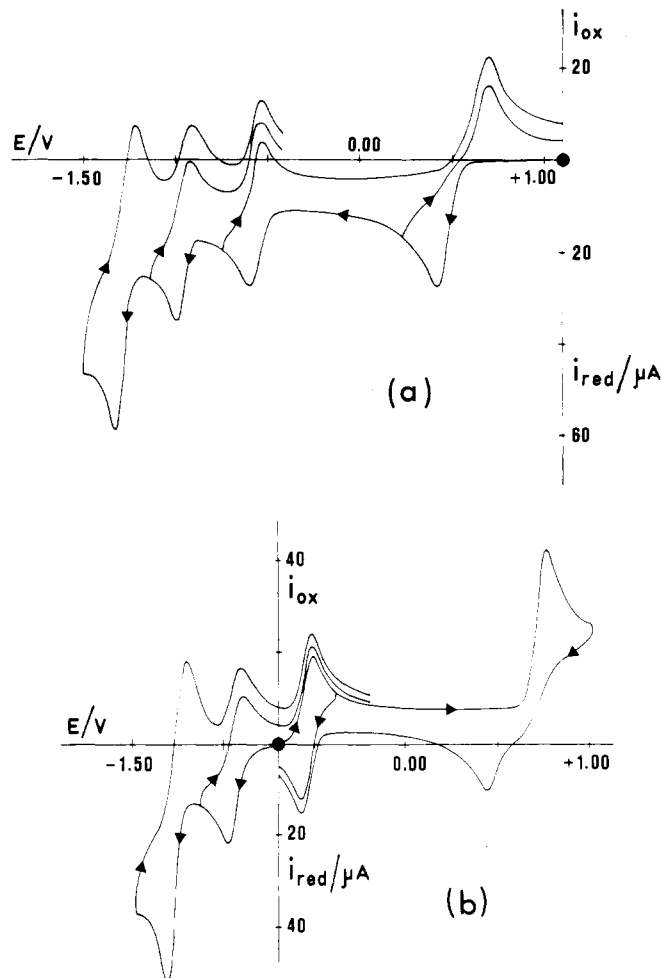


Figure 5. Cyclic voltammograms recorded on MeCN solutions of [(triphos)Rh(μ - C_2S_4)Rh(triphos)](PF $_6$) $_2$ after exhaustive electrolysis at a platinum gauze macroelectrode at: +1.0 V (a); -0.7 V (b); (NEt $_4$)ClO $_4$ (0.1 mol dm^{-3}) supporting electrolyte. Platinum working electrode. Scan rate 0.2 V s^{-1} ; (●) starting potential.

reduction processes, which, in cyclic voltammetry, appear as peaks located at -1.12 and -1.39 V in the cathodic scan and at $+0.35$, $+0.63$, and $+1.02 \text{ V}$ in the anodic scan. By reversing the direction of the scan, no peak is observed which can be directly associated to these processes, also at very high scan rates. Analogously, the triphos ligand gives rise only to an irreversible multielectron oxidation process at ca. $+1 \text{ V}$.

The electrochemical behavior of [(triphos)Rh(μ - C_2S_4)Rh(triphos)] $^{2+}$ in CH_2Cl_2 solution is similar to that observed in MeCN, with minor shifts of the redox potentials. The following formal electrode potentials have been computed for the involved charge transfers: $4+/2+$ at $+1.01 \text{ V}$, $2+/1+$ at -0.42 V , $1+/0$ at -0.85 V , and $0/2-$ at -1.30 V . These results offer the opportunity to compare the redox behavior of [(triphos)Rh(μ - C_2S_4)Rh(triphos)] $^{2+}$ with that of (η^5 -C $_5$ Me $_5$)Ni(μ - C_2S_4)Ni(η^5 -C $_5$ Me $_5$) reported by Dahl et al.^{4a} The latter compound exhibits in CH_2Cl_2 solution the following one-electron quasireversible redox processes: $1+/0$ at $+0.09 \text{ V}$, $0/1-$ at -0.92 V , and $1-/2-$ at -1.43 V .

Since **13** exhibits physical and chemical properties almost identical with its selenium analogue [(triphos)Rh(μ - C_2Se_4)Rh(triphos)](PF $_6$) $_2$ (**14**), we have also tested the redox behavior of the latter dication. As it is shown in Figure 6, the C_2Se_4 derivative gives rise to a voltammogram picture qualitatively similar to that of the sulfur analogue. The major difference is relative to the $0/-2$ charge transfer which now occurs through two one-electron steps at different potentials for the selenium derivative. At platinum electrodes, the $1-/2-$ charge transfer has the typical features of irreversibility, whereas at a mercury electrode also this step appears as a quasireversible charge-transfer located at a

(21) Tulyathan, B.; Geiger, W. E. J. Am. Chem. Soc. 1985, 107, 5960 and references therein.

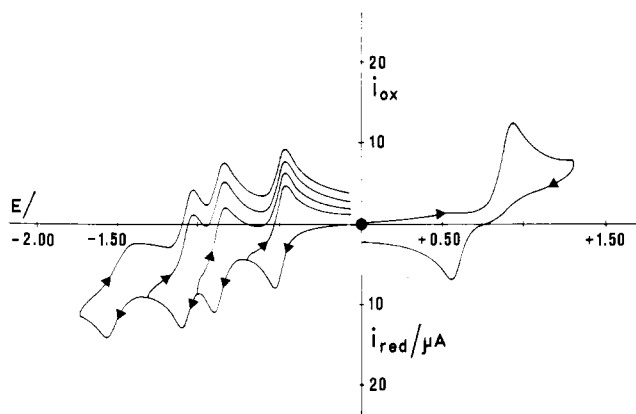


Figure 6. Cyclic voltammogram recorded on a platinum electrode from a MeCN solution containing $[(\text{triphos})\text{Rh}(\mu\text{-C}_2\text{S}_4)\text{Rh}(\text{triphos})](\text{PF}_6)_2$ (5.0×10^{-4} mol dm $^{-3}$). Scan rate 0.2 V s $^{-1}$: (●) starting potential.

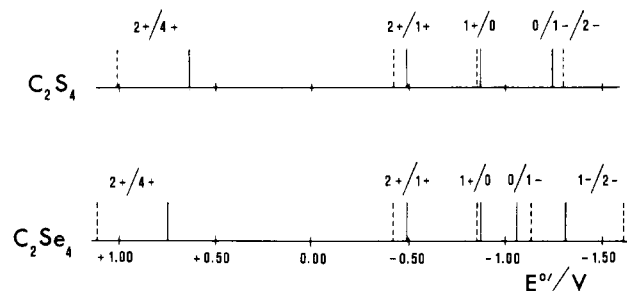
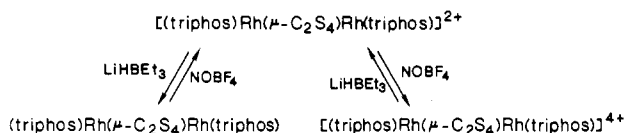


Figure 7. Schematic representation of the redox potentials (in V vs. SCE) of $[(\text{triphos})\text{Rh}(\mu\text{-C}_2\text{S}_4)\text{Rh}(\text{triphos})]^{2+}$ and $[(\text{triphos})\text{Rh}(\mu\text{-C}_2\text{Se}_4)\text{Rh}(\text{triphos})]^{2+}$ in MeCN (—) and CH $_2$ Cl $_2$ (---) solvents.

Chart I

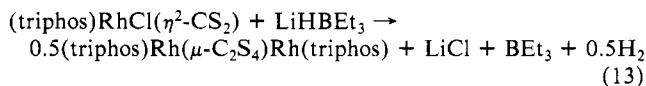


formal electrode potential of -1.31 V.

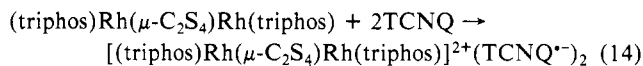
Finally, Figure 7 reports a schematic diagram of the redox potentials for $[(\text{triphos})\text{Rh}(\mu\text{-C}_2\text{S}_4)\text{Rh}(\text{triphos})]^{2+}$ and $[(\text{triphos})\text{Rh}(\mu\text{-C}_2\text{Se}_4)\text{Rh}(\text{triphos})]^{2+}$. Interestingly, it seems that solvation effects play a negligible role on the energy differences between the different redox changes. Hence, on the basis of the thermodynamic redox potentials, it is possible to calculate a difference of ca. 0.4 eV between the energy levels which may host the first and second electron added in the order to $[(\text{triphos})\text{Rh}(\mu\text{-C}_2\text{X}_4)\text{Rh}(\text{triphos})]^{2+}$. We may also speculate that the difference in energy between the LUMO and HOMO orbitals is 1.25_{av} eV for the $[\mu\text{-C}_2\text{S}_4]^{2+}$ compound and 1.35_{av} eV for the $[\mu\text{-C}_2\text{Se}_4]^{2+}$ derivative. In a following section, the relevant electrochemical results will be interpreted in terms of the electronic structure of the species as resulting from a MO analysis.

Redox Chemistry and Electron-Transfer Reactions. In agreement with the results of the electrochemical studies, it can be shown that $[(\text{triphos})\text{Rh}(\mu\text{-C}_2\text{S}_4)\text{Rh}(\text{triphos})]^{2+}$ can be chemically reduced and oxidized without destroying its dimeric framework (Chart I).

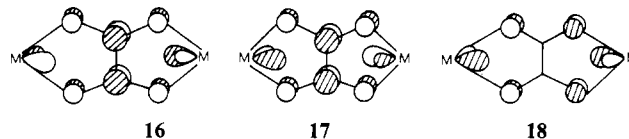
Reduction of **7** by LiHBEt $_3$ or NaBH $_4$ gives the neutral complex $(\text{triphos})\text{Rh}(\mu\text{-C}_2\text{S}_4)\text{Rh}(\text{triphos})$ (**15**), which is paramagnetic with a magnetic moment corresponding to two unpaired spins ($\mu_{\text{eff}} = 3.20 \mu_B$). Interestingly, **15** can be obtained in a one-step reaction by treatment of the starting $\eta^2\text{-CS}_2$ complex **1** with NaBH $_4$ or LiHBEt $_3$ (eq 13). The presence of both a Lewis acid and a



reducing agent in NaBH $_4$ and LiHBEt $_3$ is critically important for promoting the reaction. In particular, notice that (PPN)BH $_4$ or (NBu $_4$)BH $_4$ fail to convert **1** to **15**. Compound **15**, stable in the solid state and in solution under an inert atmosphere, is rapidly oxidized by atmospheric oxygen or by NOBF $_4$ in CH $_2$ Cl $_2$ solution to give the diamagnetic 2+ derivative (see Chart I). Complex **15** has a high tendency to transfer electrons to an acceptor substrate as shown by the easy reaction with 7,7,8,8-tetracyanoquinodimethane, TCNQ (**12**), to form the compound $[(\text{triphos})\text{Rh}(\mu\text{-C}_2\text{S}_4)\text{Rh}(\text{triphos})]^{2+}(\text{TCNQ}^{\cdot-})_2$ (**16**) (eq 14).



Compound **16** is paramagnetic with $\mu_{\text{eff}} = 2.70 \mu_B$. The ESR spectrum displays a single symmetrical signal with a g value of 2.0025 indicating that the paramagnetism arises from the organic radicals. Unfortunately, **16** does not conduct electricity. However, this fact by itself does not exclude the possibility that $[\text{M}(\mu\text{-C}_2\text{S}_4)\text{M}]^{n+}$ cores may be used to prepare new materials with metallic properties.



Oxidation of **7** by NOBF $_4$ in CH $_2$ Cl $_2$ yields the diamagnetic complex $[(\text{triphos})\text{Rh}(\mu\text{-C}_2\text{S}_4)\text{Rh}(\text{triphos})](\text{BF}_4)_4$ (**17**). Compound **17** is air-stable in the solid state and in solution, in which it behaves as a 1:4 electrolyte. Infrared and $^{31}\text{P}\{^1\text{H}\}$ NMR spectroscopic data provide useful information on the structure of **17**. A strong C=S stretching vibration at 1000 cm $^{-1}$ and the magnetic nonequivalence of the three phosphorus atoms of triphos strongly suggest a conformational variation in the dimeric framework as well as in the electronic nature of the bridging C $_2$ S $_4$ ligand. In fact, recall that no C=S stretching vibration is observed in the IR spectrum of **10** and that its $^{31}\text{P}\{^1\text{H}\}$ NMR spectrum consists of a singlet. Conversely, the $^{31}\text{P}\{^1\text{H}\}$ NMR spectrum of **17** (CD $_2$ Cl $_2$, 293 K) exhibits an AB $_2$ X pattern with δ A 19.72 ($J_{\text{A-B}} = 30$ Hz, $J_{\text{A-Rh}} = 104$ Hz) and δ B 0.42 ($J_{\text{B-Rh}} = 85.3$ Hz). Such a ^{31}P NMR pattern is suggestive of the nonequivalence of the three phosphorus atoms of each triphos around the metal centers, hence of the existence of a conformational barrier for the relative orientation of the bridging C $_2$ S $_4$ unit with respect to the L $_6$ M $_2$ grouping (this point is discussed in terms of MO theory in the next section). On the other hand, the appearance of a strong $\nu(\text{C}=\text{S})$ indicates that the two-electron oxidative process affects the bridging ligands at a large extent. Accordingly, the C $_2$ S $_4$ ligand, which has the ethenetetrathiolate structure in **7**, might become closer to a tetrathiooxalate group in **17**.

In agreement with the reversibility of the electrochemical process, **17** is able to give back the 2+ derivative by a chemical addition of two electrons. In particular, the two electrons can be extracted from tetrathiafulvalene, TTF, to give $[(\text{triphos})\text{Rh}(\mu\text{-C}_2\text{S}_4)\text{Rh}(\text{triphos})](\text{BF}_4)_2$ (**18**) and the salt $(\text{TTF})_3(\text{BF}_4)_2$ (eq 15).²³

$$\begin{array}{l}
 [(\text{triphos})\text{Rh}(\mu\text{-C}_2\text{S}_4)\text{Rh}(\text{triphos})](\text{BF}_4)_4 + 3\text{TTF} \rightarrow \\
 [(\text{triphos})\text{Rh}(\mu\text{-C}_2\text{S}_4)\text{Rh}(\text{triphos})](\text{BF}_4)_2 + (\text{TTF})_3(\text{BF}_4)_2 \\
 (15)
 \end{array}$$

Although the electrochemical studies indicate a great stability for the monocationic dimer $[(\text{triphos})\text{Rh}(\mu\text{-C}_2\text{S}_4)\text{Rh}(\text{triphos})]^+$, we have not been able to isolate it chemically. However, $[(\text{triphos})\text{Rh}(\mu\text{-C}_2\text{S}_4)\text{Rh}(\text{triphos})](\text{ClO}_4)$ (**19**) has been electrogenerated by macroelectrolysis at controlled potential. Compound **19** is paramagnetic with a magnetic moment corresponding to one unpaired spin ($\mu_{\text{eff}} = 2.04 \mu_B$).

All of the results presented in this and in the preceding section point out the noticeable electron-transfer properties of this family

(22) Sato, T.; Inoue, M.; Inoue, M. B.; Nakamura, D. *Bull. Chem. Soc. Jpn.* **1983**, *56*, 1903.

(23) Wudl, F. *J. Am. Chem. Soc.* **1975**, *97*, 1962.

to two CS₂ molecules takes place through a very specific mechanism of *electron jumping*. Conversely, the π_{\perp} bonding interaction, $1b_u-2b_u$, is of the donor-acceptor type, and it promotes the formation of the C-C π bond through a widespread electron delocalization. The *noninnocent* character of the C₂S₄ ligand becomes transparent. Perturbation theory arguments suggest the assignment of the bonding electrons to the FMO lower in energy.²⁸ Here the relative order is not clearly definable not only because of the poor reliability of the extended Hückel method but also because the energy of the ligand's FMO $2b_u$ depends on the length of the C-C linkage. Suppose that initially the two electrons of the HOMO belong to the metals (as it may be the case): the stronger the $1b_u-2b_u$ interaction, the more electron density accumulates on the latter C₂S₄ orbital, the shorter becomes the C-C bond, the lower in energy the FMO $2b_u$ itself. At this point this assignment of two electrons to the bridging ligand or to the two metals becomes only a matter of formalism. In the former case an ethenetetrathiolate ligand would donate a total of six electron pairs (four σ and 2π) to two d⁶ metals, in the latter case, the ligand would donate only five electron pairs, while a sort of backdonation from two d⁷ metals promotes the formation of a C=C bond in C₂S₄. Our favored description is that of two d⁷ metal ions which couple their spins through the delocalized π system of the ligand. In this sense the bridge favors a type of *superexchange* interaction which quenches the paramagnetism. This aspect has been treated for μ -oxalato bridged dimers.²⁹ However, the π_{\perp} system of C₂O₄ is much less engaged than that of C₂S₄, as computationally²⁹ and experimentally³⁰ shown.

The coplanarity of the Rh(μ -C₂S₄)Rh core is not a requisite for π delocalization in SQ dimers. The asymmetry of the d_{π} lobes (FMO S in **15**) with respect to the C₂S₄ plane is responsible for the flipping of the metal above and below such a plane. In fact, we suggest that the asymmetric overlap with the lobes of sulfur p_{π} orbitals (see **16**) is the driving force for this trend. Alvarez, Vicente, and Hoffmann²⁵ have optimized the flipping of L₃M moieties, and their quantitative results are consistent with the observed 0.3 Å deviation of the rhodium atoms from the C₂S₄ plane in complex **10**.

The π^* MOs $2a_g$ and $2b_u$ are calculated about 1.8 eV above $1b_u$ and about 0.4 eV from each other. Such a level ordering and its energetics are consistent with the electrochemical data reported in a previous section. Four electrons can be gradually added into the MOs $2a_g$ and $2b_u$. Two one-electron reversible cathodic processes are indicative of the formation of paramagnetic species. In particular, uncharged and monovalent dimers can be isolated. The proximity of the high lying π^* levels accounts for the triplet and doublet ground states of these two species. At this point, we recall that the complex $[(C_5Me_5)Ni(\mu-C_2S_4)Ni(C_5Me_5)]$,^{4a} formally isoelectronic with **15**, is diamagnetic. We have already reported that the π_{\perp} interaction of a_g symmetry may not be as strong in the nickel compound on account of a large contraction of the metal orbitals.¹⁰ In this case, the $2a_g-2b_u$ gap would be larger. Interestingly, the geometry of the C₂S₄ in the nickel compound is very similar to that of the rhodium complex **10**: in the former, the two electrons populating the MO $2a_g$ are not expected to affect the geometry of the ligand, given the absence of carbon character in the FMO $2a_g$ of C₂S₄. Moreover, one of the π_{\perp} bonding interactions (a_g) between C₂S₄ and the metals is vanished. Consequently the ligand would donate only four σ electron pairs to two CpNi fragments. The other π_{\perp} bonding interaction of b_u symmetry remains active. In this case, the viewpoint of a metal π_{\perp} backdonation seems even more convincing since a formal Ni^{III} metal is a rarity. It is also noteworthy that the C-C shortening and the C-S lengthening effects are the largest in the complex $[(CO)_6Fe_2(\mu-C_2S_4)Fe_2(CO)_6]$ ^{4b} where a cooperative backdonation from four metals may be at work. For the opposite

reason the longest C-C bond is observed in the mononuclear complex $PPh_3(CO)_2Fe[S_2C_2(SMe)_2]$.¹⁸

A third and a fourth electron may be added electrochemically to complex $[(triphos)Rh(\mu-C_2S_4)Rh(triphos)]^{2+}$ in a single two-electron step at the same potential. This does not necessarily mean that the two electrons enter the same orbital and, consequently, that the features of the MO scheme are not invalidated. In fact, it is well-known that in those cases, when the second electron is microscopically easier to add than the first one, a single two-electron step takes place.²¹

Conversely, we cannot offer any reasonable explanation of the fact that the analogous system $[(triphos)Rh(\mu-C_2Se_4)Rh(triphos)]^{2+}$ takes the third and fourth electron in two one-electron steps at the same potential.

There is a good agreement between the energy gaps derivable from the calculations and the electrochemical data. For both the sulfur and selenium compounds the gap between the $2a_g$ and $2b_u$ levels is estimated ca. 0.4 eV, practically equal to the calculated one. Conversely the calculated $1b_u-2a_g$ gaps are ca. $1/3$ larger than those obtainable from electrochemical data for both types of derivatives. Interestingly, however, the electrochemical data assign a 15% larger gap to the selenium derivative, in nice agreement with the calculations. Indeed larger π_{\perp} interactions can be expected for the selenium species on account of the larger diffuseness of Se orbitals and consequently of a better overlap with the metal orbitals.

³¹P NMR data show that the six terminal phosphorus atoms in the dicationic complex $[(triphos)Rh(\mu-C_2S_4)Rh(triphos)]^{2+}$ are not distinguishable, since they give rise to a unique peak. The situation probably arises from the absence of any significant rotational barrier of the C₂S₄ ligand about the axis which connects the two metals. Extended Hückel calculations show that the energetics of the two conformations SQ and TB are very similar for an electron count corresponding to that of $[(triphos)Rh(\mu-C_2S_4)Rh(triphos)]^{2+}$.

The removal of two electrons from $[(triphos)Rh(\mu-C_2S_4)Rh(triphos)]^{2+}$ to give the oxidized species $[(triphos)Rh(\mu-C_2S_4)Rh(triphos)]^{4+}$ changes substantially the features of the NMR spectrum which shows an AB₂X pattern. It may be assumed that the phosphorus atoms of each triphos ligand do not remain equivalent for a SQ \rightarrow TB interconversion and that an energetic barrier is raised. Also, a strong $\nu(C=S)$ absorption peak appears in the region of 1000 cm⁻¹ of the IR spectrum. Unfortunately, it was not possible to grow suitable crystals of the tetracation to X-ray investigate the eventual structural rearrangement of the dimeric framework.³² However, it is possible to speculate on the electronic origin of the barrier. With the help of the diagram at the right side of Figure 8 the MO pattern for the TB geometry can be compared with that of SQ. On account of the different orientation of the molecular twofold axis with respect to the C-C bond, several levels of symmetry a become symmetry b and vice versa but not all of them. Four σ interactions remain as strong as in the SQ model, the interacting levels being $2a_g-1a_g$, $2b_u-1b_u$, $1a_g-3a_g$, and $1b_u-2b_u$. The π_{\perp} interactions are $1b_g-1b_g$ and $1a_u-2a_u$. The MO $2a_u$ is now slightly destabilized with respect to the corresponding $2b_u$ level in SQ, mainly because of the presence of a lower C₂S₄ $1a_u$ FMO. Notice that the equivalent of this latter level in SQ has also a_u symmetry, and for this reason it cannot mix with the important b_u (π_{\perp}) MOs. In $[(triphos)Rh(\mu-C_2S_4)Rh(triphos)]^{2+}$, the energy difference between the HOMOs ($2a_u$ and $2b_u$) of SQ and TB conformations is not such to introduce a rotational barrier. However, after removal of two electrons, some density can still be driven from the filled C₂S₄ $1a_u$ level into the metal π_{\perp} hybrids only in TB geometry. The interaction satisfies in part the sudden electron deficiency at the metal atoms and is at the origin of the barrier in $[(triphos)Rh(\mu-C_2S_4)Rh(triphos)]^{4+}$. The calculation provides a difference of 0.3 eV between the SQ and TB models having exactly the same Rh(μ -C₂S₄)Rh core. However the actual barrier can become larger if the TB structure is optimized. In fact, a comparison of the overlap populations for Rh-S and C-S bonds, all fixed at 2.3 and 1.7 Å, respectively, indicates additional deformational trends.

(28) Hoffmann, R. *Acc. Chem. Res.* **1971**, *4*, 1.

(29) Hay, P. J.; Thibeault, J. C.; Hoffmann, R. *J. Am. Chem. Soc.* **1975**, *97*, 4884.

(30) In fact the C-C distance in bridging oxalate ligand is close to that of C-C single bonds. See, for instance: Julve, M.; Verdager, M.; Gleizes, A.; Philoche-Levisalles, M.; Kahn, O. *Inorg. Chem.* **1984**, *23*, 3808.

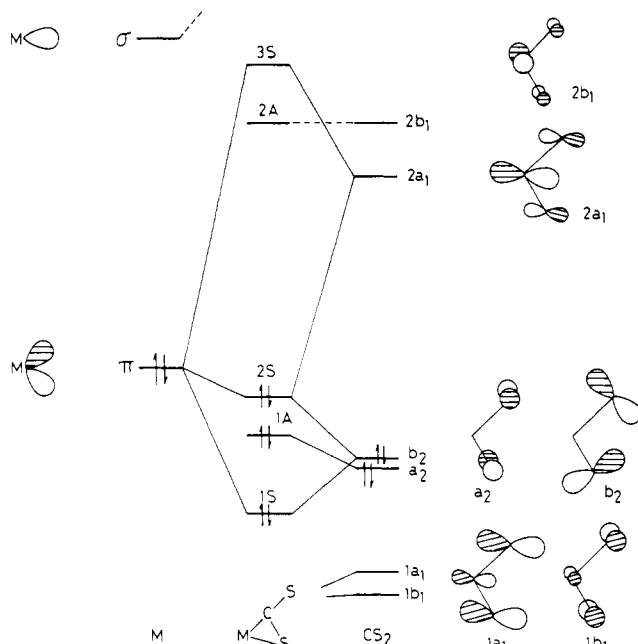


Figure 9. General diagram for the interaction of CS_2 FMOs with frontier σ and π metal orbitals.

The $Rh-S_{\text{equatorial}}$ bond becomes stronger than the $Rh-S_{\text{apical}}$ bond (overlap population 0.64 vs. 0.57). At the same time the $C-S_{\text{eq}}$ linkage becomes weaker (longer) than the $C-S_{\text{ap}}$ (overlap population 0.87 vs. 0.97 to be compared with a 0.93 value in the SQ geometry). Because of the well-known weakness of the EHMO method to evaluate precise bond distances, the optimization has not been attempted.

The trends for the overlap population suggest that the C_2S_4 ligand is assuming more tetrathiooxalate character in agreement with the appearance of the $\nu(C=S)$ stretch in the IR spectrum. When the electron density in the $2a_u$ (or $2b_u$) level of C_2S_4 is vanishing, much of the $C-S$ π antibonding disappears and double bond character is assigned to the $C-S$ linkages.³² Moreover the electron donation from the ligand's FMO $1a_u$ would originate a partial double bond between each metal and each S_{eq} atom in TB.³³ This point cannot be verified with experimental structural data, but in the monomeric complex $(PPh_3)(CO)_2Fe(C_2S_4Et_2)$ ¹⁸ the geometry of the polyhedron about iron is actually TB, and the $Fe-S_{\text{eq}}$ bond is 0.03 Å shorter than the $Fe-S_{\text{ap}}$ one.

Chemical and Theoretical Considerations on the Genesis of the C_2X_4 Ligands. The present study has shown that η^2-CS_2 and η^2-CSe_2 metal complexes are the precursors in the *head-to-head* dimerization process of heteroallene molecules. We have previously devoted considerable attention to the electronic structure of η^2-CS_2 metal complexes.⁵ Figure 9 summarizes the main bonding interactions between the FMOs of a CX_2 molecule and those of a suited metal fragment.

Substantially, almost all of the bonding between the two fragments occurs in the $M-CS_2$ plane, which, at the best, coincides

(31) Recall that the MO method used is for mono-electronic functions, whereas, during the filling of the upper levels, interelectronic effects may become quite important.

(32) A nonplanar rearrangement of the C_2S_4 ligand cannot be in principle excluded, especially if one considers that the two-electron oxidation formally transforms the C_2S_4 ligand from ethenetetrathiolate into tetrathiooxalate. A torsion at the $C-C$ single bond was observed in the uncoordinated $C_2S_4^{2-}$ molecule²⁰ and some μ -oxalate dinuclear complexes. See: Julve, M.; Verdaguer, M.; Kahn, O.; Gleizes, A.; Philoche-Levisalles, M. *Inorg. Chem.* **1983**, *22*, 368.

(33) It can be shown that the mixing between the FMOs $1a_u$ and $2a_u$ in the bonding reinforces the contribution of the p_{\perp} orbitals of the two S_{eq} atoms so that their combination becomes a π_{\perp} lone pair of some sort. Notice that in $[(\text{triphos})Rh(\mu-C_2S_4)Rh(\text{triphos})]^{2+}$ ten π_{\perp} electrons can be formally assigned to C_2S_4 (ethenetetrathiolate), four of which are shared with the metals. In $[(\text{triphos})Rh(\mu-C_2S_4)Rh(\text{triphos})]^{4+}$ there would be only eight π_{\perp} electrons in C_2S_4 , but still four of them would be used for binding the metals.

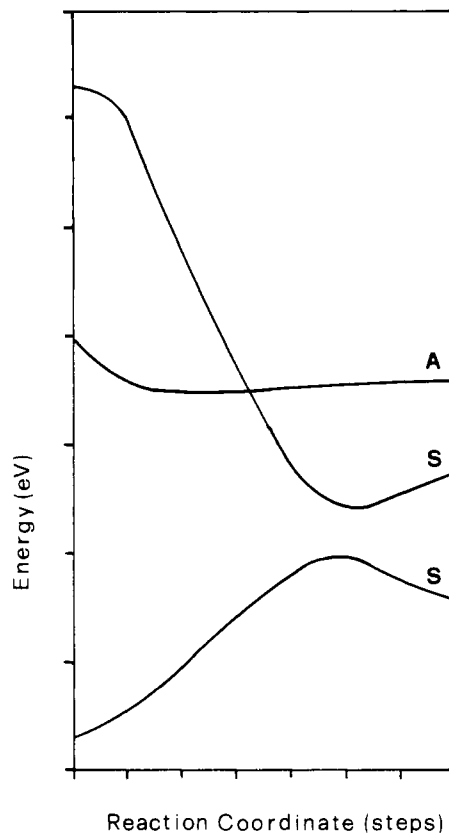


Figure 10. Evolution of the relevant MOs for the opening of the $RhSCS$ ring at the $Rh-C$ side in the $[L_4Rh(\eta^2-CS_2)]^+$ model. The abscissa refers to a discrete series of points defined by combined values of α and β (α varies in the range $60-130^\circ$, β in the range $24-0^\circ$).

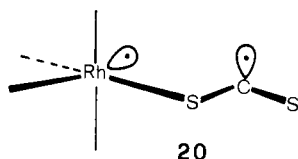
with the only symmetry element of the complex (the MOs are classified accordingly as S or A). The bent CX_2 molecule contributes with the orbitals $1a_1$, b_2 , and $2a_1$ (shown in 14), the metal with a π and a σ hybrid. In general, transition-metal fragments, which have a filled π and an empty σ level in the frontier region, are all supportive of the η^2-CS_2 coordination mode. Among these we recall $d^{10}-ML_2$, d^8-ML_4 , and $d^{10}-ML_3$ fragments. Notice that all of the five in-plane FMOs are allowed to mix. In particular the complex MO, $2S$ (most often the HOMO), is a combination of metal π and CX_2b_2 and $2a_1$ orbitals. The shape of $2S$ is shown in 19.

As seen, the atomic p orbital centered at the exocyclic sulfur atom has become large in size. Electrophiles such as H^+ , R^+ ($R = \text{alkyl}$), or even a σ electrophilic metal fragment attack here the coordinated heteroallene. Since the presence of Lewis acids enhances the rate of the reaction 6, one could infer that the opening of the $M-S-C$ ring is facilitated in $M-\eta^2-CS_2R$ complexes. Although we can anticipate that such an assumption is likely wrong, we first evaluate the theoretical chances for opening the $Rh-C$ linkage in $L_4Rh(\eta^2-CS_2)$ and in $L_4Rh(\eta^2-CS_2H)^+$ complexes.³⁴ One must follow the evolution of the three highest MOs ($2S$, $2A$, and $3S$) in Figure 9 as a function of the stretching of the $Rh-C$ bond. This may be done by opening the $Rh-S-C$ angle

(34) In our model the rhodium atom is assigned an initial d^8 electron configuration, and the four L ligands are simulated by hydride anions with the charges properly adjusted.

and by readjusting the coordination sphere at the metal. Two reasonable angular deformations are operated simultaneously: the opening α angle governs the Rh-C cleavage, and the rotation β leads to a final trigonal bipyramidal geometry about the metal, see Figure 10.

As a result, the MO 3S (LUMO) drops in energy whereas 2S (HOMO) rises. Substantially, these two orbitals are the antibonding and bonding combinations between the metal π and the CS_2 $2a_1$ FMO. No major effect is observed for the level 2A which is strongly CS_2 π^* antibonding in character but has little interaction with any metal orbital. What is interesting is that the level 3S correlates with one of the members of the $2e$ set of a trigonal bipyramid, i.e., a largely metal centered orbital, whereas 2S correlates with an orbital which is very close to that of the free CS_2 $2a_1$ level, namely the in-plane π^* level. The intended correlation leads to an avoided level crossing in a region where the metal and carbon atoms are already far away from each other (more than 3 Å). In order to avoid an intercrossing, the levels 2S and 3S mix into each other by sharing both metal and carbon character. The theory of electron transfer reactions³⁵ indicates that such a situation is potentially favoring a *sudden electron jump*. In principle, there could be a physical separation of the electrons and the formation of the diradical **20**. A torsion of CS_2 about the Rh-S bond may avoid the recombination of the electrons and ensure a finite lifetime to the triplet state. The attainment of a free radical carbon center seems to be the keystone for the formation of a new C-C bond.



The diagram of Figure 10 clearly envisages the possibility for $\text{ML}_4\text{-}\eta^2\text{-CS}_2$ to undergo an intramolecular diradical cleavage, although the process is apparently expensive in terms of energy. The two electrons, paired in 2S, are both raised in energy. Possibly in response to these energetics and Racah parameters it may be profitable to promote an electron in a higher level. The process is probably analogous to the dissociation of NaCl. It is well-known that a MO treatment leads to wrong products (Na^+ and Cl^- in place of sodium and chlorine atoms); however, the problem can be solved in a VB scheme by mixing ionic and covalent contribution to the wave function.³⁵

The protonation of the exocyclic sulfur atom does not seem to favor particularly the process. A certain stabilization of both the 2S and 3S levels ensues, but the overall MO patterns remain substantially unchanged. In actuality there is no example in which, upon the *head-to-head* dimerization of CS_2 , the supporting ML_4 ($M = d^8$) fragment is preserved. Noticeably $\text{ML}_4\text{-}\eta^2\text{-CS}_2$ is among the most stable complexes of this type.

At this point it is necessary to reconsider the role of the Lewis acid in reactions 7-10. A consistent hypothesis is that the Lewis acid labilizes the linkage between the metal and the monodentate ligand in (triphos)LRh fragments ($L = \text{Cl}, \text{N}_3$). The experimental arguments summarize as follows: (1) the $\mu\text{-C}_2\text{S}_4$ complexes **10** and **12** are quantitatively formed also by the reaction of CS_2 and CSe_2 with [(triphos)Rh(COD)] BPh_4 or with [(triphos)Rh-(C_2H_4) $_2$] BPh_4 . (ii) The formation of **7**, **8**, and **9** by addition of alcohols to CH_2Cl_2 solutions of **1**, **3**, or **4** (see eq 6) is most likely due to an increase in the polarity of the solution. It is well-known that such an effect may induce the dissociation of the chloride ions from rhodium complexes. In this context, recall that the addition of alcohols to a CH_2Cl_2 solution of (triphos)Rh(N_3)($\eta^2\text{-CS}_2$) has no consequence, whereas only the action of a strong Lewis acid, such as H^+ or CH_3^+ , converts this $\eta^2\text{-CS}_2$ precursor to the

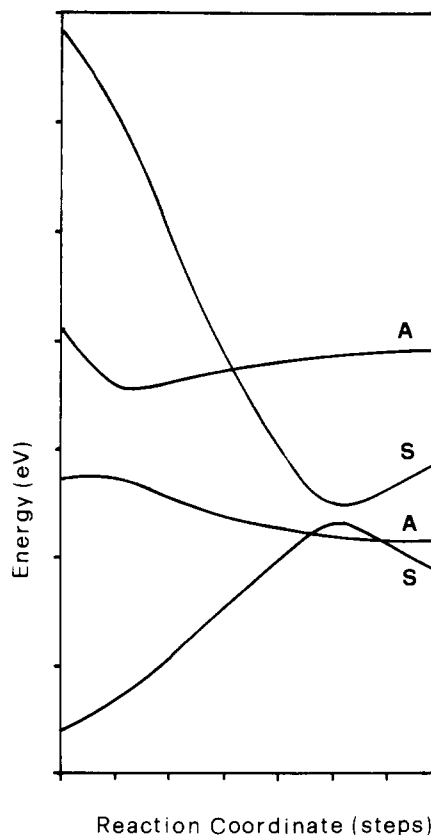
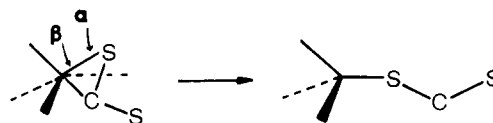
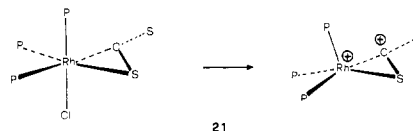


Figure 11. Evolution of the relevant MOs for the opening of the RhSCS ring at the Rh-C side in the $[\text{L}_3\text{Rh}(\eta^2\text{-CS}_2)]^+$ model. The steps in abscissa refer to combinations of α and β values in the range 60-130° and 24-0°, respectively.

dimer. The electrostatic rhodium-nitrogen (N_3) interaction is most likely stronger than that between rhodium and chlorine, so that the former is less affected by the polarity of the medium.

If the departure of the anionic ligand is taken for granted, the $d^8\text{-ML}_4$ fragment of complexes **1-4** transforms into a $d^8\text{-ML}_3$ fragment as shown in **21**. Intuitively, a major source of instability



for the $\text{ML}_3\text{-}\eta^2\text{-CS}_2$ complex originates from a larger electrostatic repulsion between rhodium and carbon atoms which ultimately promotes the Rh-C cleavage. We have previously analyzed in detail the electronic structure of $\text{ML}_3\text{-}\eta^2\text{-CS}_2$ complexes which can be stabilized for d^{10} or d^9 metals.^{5,36}

Only one of the ML_3 π hybrids, depicted in **15** is used for bonding the CS_2 molecule. The other orbital, pointing midway between the dihapto-coordinated C and S atoms, remains non-bonding (MO 1A). Its energetic position is somewhat above the MO 2S, so that for d^{10} or d^9 metals it represents the HOMO or

(35) The argument is exhaustively treated in the textbook of Salem, L. *Electrons in Chemical Reactions: First Principles*; Wiley Interscience: New York, 1982. For a more specific treatment of electron-transfer reactions concerning metal elements, see: (a) Burdett, J. K. *Inorg. Chem.* **1978**, *17*, 2537. (b) Burdett, J. K. *Comments Inorg. Chem.* **1981**, *1*, 85.

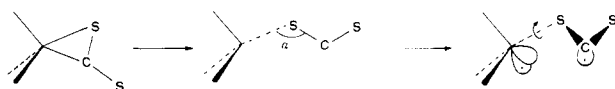
(36) Mealli, C.; Hoffmann, R.; Stockis, A. *Inorg. Chem.* **1984**, *23*, 56. Bianchini, C.; Masi, D.; Mealli, C.; Meli, A. *Inorg. Chem.* **1984**, *23*, 2838.

SOMO of the complex. For a d^8 configuration the MO 1A would be the LUMO.

Let us think now of a molecular deformation which cleaves the Rh–C bond and rearranges the overall geometry to tetrahedral. Figure 11 shows the evolution of the frontier levels as a function of the angles α and β (defined in Figure 11). The behavior of the MOs 2S and 3S parallels that already observed in the case of $L_4M(\eta^2-CS_2)$: there is an avoided crossing for a Rh–C distance larger than 3 Å. However, in $L_3M(\eta^2-CS_2)$ there are two, not one, A levels in the frontier region. The higher level 2A is $CS_2 \pi^*$ in character and is the equivalent of 2A in Figures 9 and 10. At the beginning of the pathway the two A levels mildly repel each other, and then they remain quite constant. The important point to be made is that the MO 1A remains located in the region of the avoided crossing between S orbitals also. At the tetrahedral geometry the quasidegeneracy of two metal orbitals (2S and 1A) is naturally expected (e levels). The copresence of three levels at close energies allows a competition between a diradical system and a metal-centered triplet ground state. Obviously, the pathway chosen is arbitrary, but it served to convince us that also in the presence of L_3M fragments the energetics of the levels lead to the avoided crossing.

The question is whether the attainment of other fragmental geometries may sweep the metal-centered 1A orbital away from the frontier region so that the diradical becomes favored. The search for such a geometry is complicated by the disappearance of the symmetry plane and by the consequent mixing of all of the MOs. We have found the following pathway a reasonable one.

An initial TB geometry, **22**, is assigned to the $L_3M(\eta^2-CS_2)$ complex (no significant TB–SQ barrier does exist even for the d^8 metal configuration). Then, we simultaneously promote the Rh–C cleavage, the bending of CS_2 out of the symmetry plane (the paper's plane), and the torsion of CS_2 about the Rh–S linkage. Such a complex rearrangement yields a fragment, **23**, which can



be ideally derived from a square pyramid after removal of one basal ligand (that is cis to the sulfur atom). The fragment **23**, which is geometrically suited to dimerize giving the final structure of complex **10**, has two metal hybrids, one empty pointing toward the missing basal ligand and one half-populated in a trans axial position. The former orbital correlates with the metal d_{π} hybrid 1A and actually is a new hybrid between that orbital and a higher lying $L_3M \sigma$ hybrid. This orbital is also ready to receive a lone pair donated by the originally *exocyclic* sulfur atom of an equal $L_3M(\eta^2-CS_2)$ fragment. The new Rh–S interaction begins to take place when the C–C bond is formed and helps to sweep away 1A from the frontier region. On the other hand, the singly populated metal orbital is substantially the tilted L_3M FMO (S in **15**) which ultimately interacts with the π_{\perp} system of C_2S_4 (see the previous section). Through a structural reorganization of this type, the unpaired electrons on the metals, which originate from the homolytic splitting of the Rh–C σ bond, may participate to the delocalized π_{\perp} linkage with C_2S_4 .

To summarize, the perturbation theory arguments have clearly indicated that a homolytic Rh–C cleavage is inherent to the mixing of metal and carbon characters of two MO levels when they undergo an avoided crossing at a significantly long Rh–C distance. Such an effect is found for both L_4M and $L_3M d^8$ fragments. However, the required activation energy seems to be available only to the η^2-CS_2 complexes of the latter fragment on account of strong electrostatic repulsion. A reasonable pathway has been outlined which goes through the formation of diradical species. A structural rearrangement of each L_3MCS_2 moiety is needed in order to have a good geometrical and electronic match of two of these moieties.

Conclusions

The present study through an accumulation of experimental and theoretical data has shed some light on the nature of binuclear

metal complexes containing a $\mu-C_2X_4$ ($X = S, Se$) ligand and possibly on their genesis from η^2-CX_2 complexes. The C_2S_4 ligand is stabilized on account of the formation of a C=C double bond, the required two σ and two π electrons being drained from the metals. We have indicated that, whereas the two σ electrons are captured, one from each metal, through an actual charge-transfer mechanism, the π electrons are simply delocalized through the Rh($\mu-C_2S_4$)Rh core. The latter electrons lie at the frontier region and are actually labile. In addition, other two metal–ligand π_{\perp} combinations lie at accessible energies. Ultimately, the rich electrochemistry and electron transfer properties exhibited by the series of complexes can be justified by the unique nature of the frontier MOs.

Experimental Section

All the reactions and manipulations were routinely performed under a nitrogen atmosphere. The compounds $[RhCl(C_2H_4)_2]_2$,³⁷ $[RhN_3(CO-D)]_2$,³⁸ $[IrCl(COD)]_2$,³⁹ $[(\text{triphos})Rh(COD)]BPh_4$,¹⁷ and $[(\text{triphos})Rh(C_2H_4)_2]BPh_4$ ¹⁷ were prepared according to published procedures. All materials were of reagent grade quality and were used without further purification. THF was dried over $LiAlH_4$, benzene over sodium, dichloromethane, and acetonitrile over P_2O_5 ; the solvents were purged with nitrogen and distilled immediately before use. Tetraethylammonium perchlorate and tetrabutylammonium perchlorate supporting electrolytes were dried in a vacuum oven and used without purification. The solid complexes were collected on a sintered glass frit, appropriately washed and finally dried in a stream of nitrogen. Infrared spectra were recorded on a Perkin-Elmer 283 spectrophotometer as Nujol mulls between KBr plates. $^{31}P\{^1H\}$ NMR spectra were recorded on a Varian CFT 20 spectrometer. The chemical shifts are downfield (+) from external H_3PO_4 . Conductivity measurements were made on a KTW Model LBR/B conductivity bridge in ca. 10^{-3} M nitroethane solutions. Magnetic susceptibilities of solid samples were measured on a Faraday balance. Polycrystalline powder EPR spectra were recorded at room temperature with a X-band Varian E-9 spectrometer. Electrochemical techniques were carried out by using a PAR Model 170 electrochemistry system as polarizing unity; the recording device for potential scan rates higher than 0.5 Vs^{-1} was a Hewlett-Packard Model 1123 A storage oscilloscope. Cyclic voltammetry and chronoamperometry were performed in a three-electrode cell having a platinum working electrode surrounded by a platinum-spiral counter electrode and the reference electrode mounted with a Luggin capillary. Controlled potential coulometry tests were performed in a H-shaped cell with anodic and cathodic compartments separated by a sintered glass disc. The working macroelectrode was either a mercury pool or a platinum gauze. A mercury pool was used as counter electrode. In these tests an Amel potentiostat Model 551, with an associated coulometer Amel integrator Model 558, was used. In all electrochemical tests, an aqueous saturated calomel electrode (SCE) was used as reference electrode. The temperature was controlled at $293 \pm 0.1 \text{ K}$.

(triphos)RhCl(η^2-CS_2)- C_6H_6 (1). Carbon disulfide vapors were bubbled through a mixture of $[RhCl(C_2H_4)_2]_2$ (0.58 g, 1.5 mmol) and triphos (1.87 g, 3 mmol) in benzene (150 mL). The color changed immediately from yellow-orange to red, and a gummy precipitate began to separate. This was transformed into red crystals by heating the mixture up to the boiling temperature. It was filtered and washed with benzene and petroleum ether: yield 90%. Anal. Calcd for $C_{48}H_{45}ClP_3RhS_2$: C, 62.85; H, 4.94; Rh, 11.21; S, 6.99. Found: C, 62.68; H, 4.87; Rh, 11.08; S, 6.88.

(triphos)RhN₃(η^2-CS_2) (2). Carbon disulfide vapors were bubbled through a mixture of $[RhN_3(COD)]_2$ (0.12 g, 0.25 mmol) and triphos (0.31 g, 0.5 mmol) in benzene (30 mL). When the solution became cloudy, it was gently warmed up to ca. 40 °C, and liquid carbon disulfide (5 mL) was added. Within a few minutes red-orange crystals precipitated which were filtered off and washed as above: yield 55%. Anal. Calcd for $C_{42}H_{39}N_3P_3RhS_2$: C, 59.64; H, 4.64; N, 4.96; Rh, 12.16. Found: C, 59.31; H, 4.71; N, 4.88; Rh, 11.97.

(triphos)IrCl(η^2-CS_2) (3). Carbon disulfide (10 mL) was added to a solution of $[IrCl(COD)]_2$ (0.34 g, 0.5 mmol) and triphos (0.62 g, 1 mmol) in benzene (30 mL), and the resulting yellow solution was refluxed for 2 h. Yellow crystals precipitated on cooling the solution to room temperature. They were filtered off and washed as above: yield 65%.

(37) Cramer, R. *Inorg. Synth.* **1974**, *15*, 14.

(38) La Monica, G.; Monti, C.; Pizzotti, M.; Cenini, S. *J. Organomet. Chem.* **1983**, *241*, 241.

(39) Herde, J. L.; Lambert, J. C.; Senoff, C. V. *Inorg. Synth.* **1974**, *15*, 18.

Table III. Summary of Crystal Data

compd	4	10 ·CH ₂ Cl ₂
formula	C ₄₈ H ₄₅ ClP ₃ RhSe ₂	C ₁₃₃ H ₁₂₆ B ₂ Cl ₂ P ₆ Rh ₂ S ₄
mol wt	1011.09	2286.9
cryst size, mm	0.325 × 0.15 × 0.075	0.70 × 0.175 × 0.14
space group	P2 ₁ /n	P2 ₁ /a
<i>a</i> , Å	21.151(6)	15.496(4)
<i>b</i> , Å	16.450(5)	28.736(7)
<i>c</i> , Å	13.500(3)	14.216(4)
β, deg	90.81(3) ^o	106.02(2) ^o
<i>V</i> , Å ³	4697	6084
<i>Z</i>	4	2
<i>d</i> _{calcd} , g·cm ⁻³	1.43	1.25
(Mo Kα), cm ⁻¹	20.02	5.08
radiatn	graphite-monochromated Mo Kα(λ = 0.71069 Å)	
scan type		ω/2θ
2θ range, deg	5–40	5–45
scan width, deg	1.00	1.00
scan speed, deg s ⁻¹	0.05	0.05
total data	4803	8502
unique data, <i>I</i> ≥ 3σ(<i>I</i>)	1904	2912
no. of params	191	252
<i>R</i>	0.077	0.085
<i>R</i> _w	0.082	0.088
<i>w</i> = 1.0[σ ² (<i>F</i> _o) + <i>pF</i> _o ²] ⁻¹	0.008	0.002

Anal. Calcd for C₄₂H₃₉ClIrP₃S₂: C, 54.33; H, 4.23; Ir, 20.70. Found: C, 54.18; H, 4.15; Ir, 20.52.

(triphos)RhCl(η²-CSe₂)·C₆H₆ (**4**). Neat CSe₂ (0.25 g, 1.5 mmol) was pipetted into a solution of [RhCl(C₂H₄)₂]₂ (0.1 g, 0.25 mmol) and triphos (0.31 g, 0.5 mmol) in benzene (50 mL). Immediately the solution became cloudy, and a brown orange precipitate formed. This was transformed by heating into red crystals which were filtered off and washed as above: yield 60%. Anal. Calcd for C₄₈H₄₅ClP₃RhSe₂: C, 57.01; H, 4.48; Rh, 10.17; Se, 15.61. Found: C, 56.96; H, 4.46; Rh, 10.03; Se, 15.28.

[(triphos)Rh(μ-C₂X₄)Rh(triphos)]Cl₂ [X = S (**7**); X = Se (**9**)]. Addition of ethanol (10 mL) to a red-orange solution of **1** or **4** (0.5 mmol) in CH₂Cl₂ (15 mL) caused an immediate color change to green. On addition of *n*-butyl ether (15 mL) and slow evaporation of the solvent green crystals were obtained. They were filtered off and washed with a 1:1 mixture of ethanol/*n*-butyl ether and petroleum ether: yield 85% and 75%, respectively. Anal. Calcd for C₈₄H₇₈Cl₂P₆Rh₂S₄: C, 60.11; H, 4.68; Rh, 12.26; S, 7.64. Found: C, 60.03; H, 4.61; Rh, 12.13; S, 7.49. Anal. Calcd for C₈₄H₇₈Cl₂P₆Rh₂Se₄: C, 54.06; H, 4.21; Rh, 11.02; Se, 16.92. Found: C, 54.13; H, 4.23; Rh, 10.92; Se, 16.87.

[(triphos)Ir(μ-C₂S₂)Ir(triphos)]Cl₂ (**8**). This blue complex was prepared as above except for substitution of **3** for **1**: yield 80%. Anal. Calcd for C₈₄H₇₈Cl₂Ir₂P₆S₄: C, 54.33; H, 4.23; Ir, 20.70; S, 6.90. Found: C, 54.25; H, 4.21; Ir, 20.57; S, 6.78.

Methatetical Reactions of 7, 8, and 9 with NaBPh₄. NaBPh₄ (0.17 g, 0.5 mmol) in ethanol (30 mL) was added to a solution of **7**, **8**, or **9** (0.25 mmol) in acetone (20 mL). On slow evaporation of the solvent the corresponding tetraphenylborate derivatives [(triphos)Rh(μ-C₂S₂)Rh(triphos)](BPh₄)₂ (**10**), [(triphos)Ir(μ-C₂S₂)Ir(triphos)](BPh₄)₂ (**11**), and [(triphos)Rh(μ-C₂Se₂)Rh(triphos)](BPh₄)₂ (**12**) precipitated in 90% yield: Λ_M = 102, 100, 99 cm² Ω⁻¹ mol⁻¹ for **10**, **11**, and **12**, respectively. Anal. Calcd for C₁₃₂H₁₁₈B₂P₆Rh₂S₄: C, 70.59; H, 5.29; Rh, 9.16; S, 5.71. Found: C, 70.41; H, 5.19; Rh, 9.04; S, 5.66. Anal. Calcd for C₁₃₂H₁₁₈B₂Ir₂P₆S₄: C, 65.39; H, 4.90; Ir, 15.85; S, 5.28. Found: C, 65.47; H, 4.78; Ir, 15.74; S, 5.14. Anal. Calcd for C₁₃₂H₁₁₈B₂P₆Rh₂Se₄: C, 65.14; H, 4.88; Rh, 8.45; Se, 12.97. Found: C, 65.05; H, 4.75; Rh, 8.17; Se, 13.02. Crystals of 10·CH₂Cl₂ were obtained by recrystallization of **10** in CH₂Cl₂/ethanol.

Reactions of [(triphos)Rh(COD)]BPh₄ and [(triphos)Rh(C₂H₄)₂]BPh₄ with CS₂ or CSe₂. Neat CS₂ or CSe₂ (5 and 0.5 mL, respectively) was added to a solution of [(triphos)Rh(COD)]BPh₄ (0.23 g, 0.2 mmol) or [(triphos)Rh(C₂H₄)₂]BPh₄ (0.22 g, 0.2 mmol) in THF (30 mL). After stirring for 30 min, green crystals of **10** or **12** precipitated from the resulting solutions: yield 80%.

Reaction of 1, 2, 3, and 4 with HSO₃CF₃, HBF₄, and MeSO₃CF₃. An equimolar amount of HSO₃CF₃, HBF₄, or MeSO₃CF₃ was added to a solution of **1**, **2**, **3**, or **4** (0.5 mmol) in CH₂Cl₂ (10 mL). Addition of NaBPh₄ (0.17 g, 0.5 mmol) in ethanol (20 mL) gave crystals of **10**, **11**, and **12** in 75–85% yield, respectively.

Reaction of 1, 3, and 4 with TlPF₆ or AgBF₄. TlPF₆ or AgBF₄ (0.5 mmol) was added to a stirred suspension of **1**, **3**, or **4** (0.5 mmol) in THF

Table IV. Final Positional and Thermal Parameters of (triphos)RhCl(η²-CSe₂)·C₆H₆^a

atom	<i>x</i>	<i>y</i>	<i>z</i>	<i>U</i> (Å ²)
Rh1	3208 (1)	6210 (1)	2967 (2)	35 (1)
Se1	3807 (2)	4893 (2)	3091 (2)	61 (1)
Se2	3244 (2)	4888 (2)	797 (2)	61 (1)
Cl1	2281 (3)	5402 (4)	3348 (6)	59 (3)
P1	3159 (3)	6919 (4)	4532 (5)	41 (3)
P2	4113 (3)	6890 (4)	2641 (5)	37 (3)
P3	2639 (3)	7283 (4)	2250 (5)	36 (3)
C1	3395 (13)	5309 (18)	1935 (22)	64 (9)
C2	3586 (12)	7897 (15)	4437 (18)	41 (7)
C3	3988 (12)	8004 (15)	2619 (19)	42 (7)
C4	2787 (11)	8215 (15)	2967 (18)	39 (7)
C5	3482 (11)	8311 (15)	3414 (18)	34 (7)
C6	3614 (14)	9244 (18)	3502 (23)	66 (9)
C11	2408 (12)	7228 (13)	5106 (15)	43 (7)
C21	1828 (12)	6901 (13)	4804 (15)	110 (13)
C31	1275 (12)	7132 (13)	5279 (15)	143 (17)
C41	1302 (12)	7690 (13)	6057 (15)	91 (11)
C51	1882 (12)	8017 (13)	6359 (15)	120 (15)
C61	2435 (12)	7786 (13)	5884 (15)	107 (13)
C12	3515 (8)	6420 (11)	5603 (13)	41 (7)
C22	3399 (8)	5589 (11)	5694 (13)	62 (9)
C32	3617 (8)	5169 (11)	6529 (13)	81 (10)
C42	3951 (8)	5580 (11)	7273 (13)	83 (11)
C52	4067 (8)	6412 (11)	7182 (13)	96 (12)
C62	3849 (8)	6832 (11)	6347 (13)	69 (10)
C13	4510 (8)	6675 (9)	1489 (14)	36 (7)
C23	4428 (8)	7157 (9)	646 (14)	62 (9)
C33	4749 (8)	6966 (9)	-219 (14)	76 (10)
C43	5151 (8)	6295 (9)	-242 (14)	77 (10)
C53	5233 (8)	5814 (9)	601 (14)	65 (9)
C63	4912 (8)	6004 (9)	1467 (14)	60 (9)
C14	4781 (8)	6785 (10)	3528 (11)	38 (7)
C24	5297 (8)	7291 (10)	3363 (11)	50 (8)
C34	5824 (8)	7259 (10)	3995 (11)	69 (9)
C44	5834 (8)	6720 (10)	4793 (11)	60 (9)
C54	5317 (8)	6214 (10)	4958 (11)	64 (9)
C64	4791 (8)	6246 (10)	4326 (11)	56 (8)
C15	2778 (9)	7565 (11)	976 (14)	52 (8)
C25	2728 (9)	8368 (11)	652 (14)	60 (9)
C35	2794 (9)	8552 (11)	-350 (14)	91 (12)
C45	2911 (9)	7932 (11)	-1028 (14)	71 (10)
C55	2961 (9)	7129 (11)	-705 (14)	101 (12)
C65	2895 (9)	6945 (11)	297 (14)	83 (11)
C16	1785 (9)	7168 (10)	2194 (14)	48 (8)
C26	1549 (9)	6483 (10)	1705 (14)	61 (9)
C36	898 (9)	6383 (10)	1575 (14)	72 (10)
C46	483 (9)	6970 (10)	1934 (14)	79 (11)
C56	719 (9)	7655 (10)	2422 (14)	76 (10)
C66	1370 (9)	7754 (10)	2552 (14)	62 (9)
C17	3331 (22)	221 (27)	6095 (31)	67 (18)
C27	2987 (22)	353 (27)	6955 (31)	124 (30)
C37	3303 (22)	455 (27)	4861 (31)	128 (30)
C47	3961 (22)	423 (27)	7907 (31)	91 (23)
C57	4305 (22)	291 (27)	7048 (31)	100 (25)
C67	3989 (22)	189 (27)	6142 (31)	110 (26)
C7 ^b	582 (20)	4787 (30)	4604 (34)	115 (14)
C8 ^b	307 (30)	4313 (37)	5299 (47)	183 (22)
C9 ^b	328 (32)	5503 (41)	4288 (44)	188 (22)

^a Coordinates multiplied by 10⁴, temperature factors by 10³. Temperature factors for Rh, Se, Cl and P1–P3 atoms are given as *U*(eq.). ^b Atoms define independent part of the solvent benzene molecule. The remaining atoms of the ring are related by symmetry center. Atoms of the solvent molecule (C17–C67) refined with occupancy 0.5.

(50 mL). TiCl₄ (AgCl) was then eliminated by filtration. Addition of NaBPh₄ (0.17 g, 0.5 mmol) and ethanol (10 mL) to the resulting deeply colored solution gave crystals of **10**, **11**, and **12**, respectively.

Reaction of 1, 3, and 4 with NaBPh₄. Solid NaBPh₄ (0.17 g, 0.5 mmol) was added to a suspension of **1**, **3**, or **4** (0.5 mmol) in THF (70 mL). After stirring for 1 h the starting solid dissolved and crystals of **10**, **11**, and **12** began to precipitate, respectively.

[(triphos)Rh(μ-C₂X₄)Rh(triphos)](PF₆)₂ [X = S, (**13**); Se, (**14**)]. Solid (NBu₄)(PF₆) (0.39 g, 1 mmol) was added to a solution of **7** or **9** (0.5 mmol) in CH₂Cl₂ (20 mL). On addition of ethanol (40 mL) green crystals of **13** or **14** were obtained in 95% yield, respectively. Anal. Calcd for C₈₄H₇₈F₁₂P₆Rh₂S₄: C, 53.17; H, 4.14; Rh, 10.85. Found: C,

Table V. Final Positional and Thermal Parameters for $[(\text{triphos})\text{Rh}(\mu\text{-}C_2S_4)\text{Rh}(\text{triphos})](\text{BPh}_4)_2 \cdot \text{CH}_2\text{Cl}_2^a$

atom	x	y	z	U (\AA^2)	atom	x	y	z	U (\AA^2)
Rh	1087 (1)	801 (1)	1337 (1)	34 (1)	C35	958 (8)	1958 (4)	-1317 (9)	65 (6)
P1	1096 (3)	728 (2)	2911 (4)	44 (2)	C45	881 (8)	2439 (4)	-1303 (9)	62 (6)
P2	2592 (3)	989 (2)	1856 (3)	37 (2)	C55	757 (8)	2661 (4)	-477 (9)	78 (8)
P3	737 (3)	1588 (2)	1401 (3)	38 (2)	C65	710 (8)	2400 (4)	334 (9)	59 (6)
S1	1394 (3)	76 (2)	803 (4)	51 (2)	C16	-377 (8)	1733 (5)	1494 (7)	38 (5)
S2	-327 (3)	707 (2)	299 (4)	49 (2)	C26	-1084 (8)	1728 (5)	638 (7)	51 (6)
C1	1526 (13)	1250 (7)	3627 (13)	49 (8)	C36	-1954 (8)	1831 (5)	673 (7)	67 (7)
C2	2868 (12)	1369 (6)	2932 (11)	36 (7)	C46	-2117 (8)	1940 (5)	1565 (7)	71 (7)
C3	1505 (11)	1892 (7)	2414 (11)	43 (8)	C56	-1410 (8)	1945 (5)	2421 (7)	69 (7)
C4	2087 (12)	1601 (6)	3246 (13)	37 (8)	C66	-540 (8)	1842 (5)	2386 (7)	66 (7)
C5	2519 (14)	1954 (8)	4071 (13)	57 (9)	B	952 (16)	2928 (9)	5618 (19)	56 (7)
C6	-362 (11)	147 (6)	-92 (12)	34 (8)	C17	1912 (10)	3089 (5)	6490 (10)	62 (6)
C11	1755 (8)	226 (5)	3545 (9)	45 (5)	C27	2750 (10)	2933 (5)	6438 (10)	68 (7)
C21	1433 (8)	-214 (5)	3213 (9)	67 (7)	C37	3525 (10)	3065 (5)	7153 (10)	75 (7)
C31	1916 (8)	-610 (5)	3615 (9)	75 (7)	C47	3462 (10)	3354 (5)	7920 (10)	83 (8)
C41	2722 (8)	-565 (5)	4348 (9)	84 (8)	C57	2624 (10)	3510 (5)	7972 (10)	76 (7)
C51	3045 (8)	-125 (5)	4680 (9)	79 (7)	C67	1849 (10)	3378 (5)	7257 (10)	52 (6)
C61	2562 (8)	271 (5)	4278 (9)	56 (6)	C18	109 (9)	3253 (4)	5765 (10)	45 (5)
C12	-7 (12)	666 (7)	3144 (17)	79 (7)	C28	-396 (9)	3119 (4)	6393 (10)	73 (7)
C22	12 (12)	533 (7)	4093 (17)	113 (10)	C38	-1022 (9)	3425 (4)	6593 (10)	61 (6)
C32	-789 (12)	458 (7)	4337 (17)	138 (12)	C48	-1142 (9)	3866 (4)	6164 (10)	67 (7)
C42	-1610 (12)	517 (7)	3632 (17)	154 (14)	C58	-636 (9)	4000 (4)	5536 (10)	61 (6)
C52	-1628 (12)	650 (7)	2683 (17)	219 (20)	C68	-11 (9)	3694 (4)	5336 (10)	65 (7)
C62	-827 (12)	725 (7)	2439 (17)	164 (14)	C19	771 (8)	2357 (6)	5728 (11)	58 (6)
C13	3491 (7)	573 (5)	2179 (10)	49 (6)	C29	1454 (8)	2055 (6)	6216 (11)	67 (7)
C23	3668 (7)	103 (5)	2357 (10)	45 (5)	C39	1271 (8)	1583 (6)	6294 (11)	100 (9)
C33	4108 (7)	-192 (5)	2651 (10)	59 (6)	C49	406 (8)	1413 (6)	5883 (11)	101 (9)
C43	4972 (7)	-18 (5)	2767 (10)	76 (7)	C59	-277 (8)	1715 (6)	5395 (11)	107 (10)
C53	5095 (7)	451 (5)	2590 (10)	69 (7)	C69	-94 (8)	2186 (6)	5318 (11)	83 (8)
C63	4355 (7)	747 (5)	2296 (10)	75 (7)	C110	1035 (7)	3041 (5)	4485 (9)	49 (5)
C14	2908 (9)	1293 (4)	863 (11)	35 (5)	C210	1727 (7)	3304 (5)	4301 (9)	63 (6)
C24	2933 (9)	1025 (4)	53 (11)	72 (7)	C310	1700 (7)	3424 (5)	3342 (9)	69 (7)
C34	3169 (9)	1230 (4)	-731 (11)	104 (9)	C410	980 (7)	3282 (5)	2568 (9)	76 (7)
C44	3380 (9)	1702 (4)	-705 (11)	91 (8)	C510	287 (7)	3019 (5)	2753 (9)	58 (6)
C54	3356 (9)	1970 (4)	106 (11)	82 (8)	C610	315 (7)	2898 (5)	3711 (9)	59 (6)
C64	3120 (9)	1766 (4)	890 (11)	54 (6)	Cl1	850 (21)	4007 (12)	9560 (26)	260 (15)
C15	787 (8)	1916 (4)	320 (9)	43 (5)	Cl2	1419 (21)	4813 (11)	716 (25)	242 (13)
C25	911 (8)	1694 (4)	-506 (9)	45 (5)	C7	1878 (39)	4352 (21)	189 (46)	111 (20)

^aCoordinates multiplied by 10^4 , temperature factors by 10^3 . Temperature factors for Rh, P, S, and C1-C6 atoms are given as $U(\text{eq})$.

53.02; H, 4.20; Rh, 10.90. Anal. Calcd for $C_{84}H_{78}F_6P_6Rh_2Se_4$: C, 51.18; H, 3.98; Rh, 10.45. Found: C, 50.91; H, 3.87; Rh, 10.35.

(triphos)Rh($\mu\text{-}C_2S_4$)Rh(triphos) (15). A. LiHBEt_3 (1 M in THF) (0.5 mL, 0.5 mmol) was added to a solution of **7** (0.33 g, 0.2 mmol) in THF (30 mL). The originally green solution turned dark brown within a few minutes. On addition of 1-butanol and slow concentration maroon crystals were obtained. They were filtered off and washed with ethanol and petroleum ether: yield 60%.

B. LiHBEt_3 (1 M in THF) (0.4 mL, 0.4 mmol) was added to a suspension of **1** (0.23 g, 0.25 mmol) in THF (30 mL). Within a few minutes the starting solid dissolved to give a dark brown solution. Addition of 1-butanol and slow concentration gave maroon crystals: yield 55%. Anal. Calcd for $C_{84}H_{78}P_6Rh_2S_4$: C, 62.76; H, 4.89; Rh, 12.80; S, 7.97. Found: C, 62.64; H, 4.86; Rh, 12.65; S, 7.88.

Reaction of 15 with NOBF_4 . A mixture of **15** (0.32 g, 0.2 mmol) and NOBF_4 (0.04 g, 0.35 mmol) in CH_2Cl_2 (40 mL) was stirred for 15 min. During this time the color changed gradually to green. Crystals of $10\text{-CH}_2\text{Cl}_2$ precipitated by adding NaBPh_4 (0.17 g, 0.5 mmol) in ethanol (30 mL).

Reaction of 15 with TCNQ. TCNQ (0.18 g, 0.9 mmol) was added to a stirred suspension of **15** (0.48 g, 0.3 mmol) in acetonitrile (30 mL). Immediately the starting red solid dissolved and a greenish blue microcrystalline precipitate of $[(\text{triphos})\text{Rh}(\mu\text{-}C_2S_4)\text{Rh}(\text{triphos})](\text{TCNQ})_2$ (**16**) began to separate: yield 70%. Anal. Calcd for $C_{108}H_{86}N_8P_6Rh_2S_4$: C, 64.34; H, 4.30; N, 5.56; Rh, 10.20. Found: C, 64.22; H, 4.15; N, 5.60; Rh, 9.85.

$[(\text{triphos})\text{Rh}(\mu\text{-}C_2S_4)\text{Rh}(\text{triphos})](\text{BF}_4)_4$ (17). A large excess of solid NOBF_4 was added to the green solution of **7** (0.42 g, 0.25 mmol) in CH_2Cl_2 (30 mL), and the mixture was stirred for 30 min. The excess of NOBF_4 was then eliminated by filtration. Addition of *n*-hexane to the red violet filtrate gave red crystals which were filtered off and washed with a 2:1 mixture of *n*-hexane/ CH_2Cl_2 and petroleum ether: yield 65% $\Delta_M = 270 \text{ cm}^2 \Omega^{-1} \text{ mol}^{-1}$. Anal. Calcd for $C_{84}H_{78}B_4F_{16}P_6Rh_2S_4$: C, 51.61; H, 4.02; Rh, 10.52; S, 6.56. Found: C, 51.24; H, 4.15; Rh, 10.38; S, 6.33.

Reaction of 17 with LiHBEt_3 . A solution of **17** (0.39 g, 0.2 mmol) in THF (40 mL) was treated with LiHBEt_3 (1 M in THF) (0.5 mL, 0.5

mmol). Addition of 1-butanol (50 mL) and NaBPh_4 (0.34 g, 1 mmol) to the resultant solution gave green crystals of **10**: yield 75%.

Reaction of 17 with TTF. TTF (0.16 g, 0.8 mmol) was added to a stirred solution of **17** (0.39 g, 0.2 mmol) in acetonitrile (20 mL). Gradually the color changed from red violet to green. Red crystals of $(\text{TTF})_2(\text{BF}_4)_2$ precipitated on cooling the reaction mixture to 0°C , which were then filtered off. Addition of ethanol to the acetonitrile solution caused the precipitation of green crystals of $[(\text{triphos})\text{Rh}(\mu\text{-}C_2S_4)\text{Rh}(\text{triphos})](\text{BF}_4)_2$ (**18**): yield 95%. Anal. Calcd for $C_{84}H_{78}B_2F_8P_6Rh_2S_4$: C, 56.64; H, 4.41; Rh, 11.55. Found: C, 56.55; H, 4.30; Rh, 11.02.

X-ray Diffraction Studies. Crystal data for both compounds **4** and $10\text{-CH}_2\text{Cl}_2$ are summarized in Table III. A Philips PW 1100 automated four-circles diffractometer with graphite-monochromated radiation was used for the experimental work. A set of 20 high-angle reflections were used for the centering procedure of each crystal. As a general procedure, three standard reflections were collected every 2 h (no appreciable decay of intensities was observed in any case). The data were corrected for Lorentz and polarization effects. Numerical absorption corrections were applied with transmission factors ranging between 0.87–0.71 and 0.99–0.83 for **4** and $10\text{-CH}_2\text{Cl}_2$, respectively. Atomic scattering factors were those tabulated by Cromer and Waber⁴⁰ with anomalous dispersion corrections taken from reference.⁴¹ The computational work was essentially performed by using the SHELX76 system.⁴² The final *R* factors (see Table III) are somewhat higher than usual. This is in part due to the persisting disorder that affects the solvent molecules even at the later stages of refinement. However we exclude that the feature alters significantly the important chemical information which we were pursuing.

(triphos)RhCl($\eta^2\text{-CSe}_2$)- C_6H_6 (4). The structure was solved by the Patterson method and Fourier techniques. From elemental and spectroscopic analysis the stoichiometric ratio between the complex and the solvent molecules is 1:1. The structural analysis has shown that one C_6H_6

(40) Cromer, D. T.; Waber, J. T. *Acta Crystallogr.* **1965**, *18*, 104.

(41) *International Tables for Crystallography*; Kynoch Press: Birmingham, 1974; Vol. 4.

(42) Sheldrick, G. M. SHELX76, *Program for Crystal Structure Determinations*; University of Cambridge, Cambridge, 1976.

molecule lies astride an inversion center. A second molecule lies in general position. Since the thermal parameters relative to the latter C_6H_6 molecule refine to acceptable values by assuming atomic population parameters of 0.5, the ratio given above is confirmed to be correct. Rigid body models (D_{6h}) for all of the phenyl rings and the benzene molecule in general position were adopted during the least-squares refinement. The hydrogen atoms were introduced at calculated positions ($C-H = 1.0 \text{ \AA}$). Anisotropic thermal parameters were used only for the Rh, Se, P, and Cl atoms. The final difference Fourier map has the largest peak of 0.92 e/\AA^3 which appears to be a rhodium ripple. Other peaks of about 0.5 e/\AA^3 are observed in the solvent regions. Final coordinates of all the non-hydrogen atoms are reported in Table IV.

[(triphos)Rh($\mu-C_2S_4$)Rh(triphos)](BPh₄)₂·CH₂Cl₂ (10)·CH₂Cl₂. The structure was solved by the Patterson method and Fourier techniques. During the least-squares analysis Rh, S, and P atoms as well as the unique carbon atom of the centrosymmetrically related C_2S_4 ligand were allotted anisotropic temperature factors. Also, the phenyl rings were treated as rigid bodies, and the hydrogen atoms were introduced at calculated positions. The non-hydrogen atoms of CH₂Cl₂ were assigned a population parameter of 0.5 and refined accordingly. A difference map showed some peaks ($>1 \text{ e/\AA}^3$) which were attributed to disorder in the dichloromethane solvent molecule. Also, one of the phenyl rings of the ligand triphos [one of those linked to the atom P(1)] is affected by some disorder as shown by the relatively high-temperature factors. Final coordinates of all non-hydrogen atoms are reported in Table V.

Computational Details. All calculations were of the extended Hückel type⁴³ using a modified version of the Wolfsberg-Helmholz formula.⁴⁴ The parameters for the rhodium atom were the same as in ref 45. Extensive use of Fragment Molecular Orbital analysis was performed.⁴⁶ The geometry of the model [H₃Rh($\mu-C_2S_4$)RhH₃] was fixed as follows: Rh-H = 1.7 Å; H-Rh-H = 90°; C-C = 1.4 Å; C-S = 1.7 Å; S-C-C = S-C-S = 90°.

Acknowledgment. We thank Dante Masi for technical assistance with X-ray analyses.

Supplementary Material Available: Anisotropic thermal parameters for compounds 4 and 10·CH₂Cl₂ (4 pages); listing of observed and calculated structure factors (29 pages). Ordering information is given on any current masthead page.

(43) Hoffmann, R.; Lipscomb, W. N. *J. Chem. Phys.* **1962**, *36*, 2179, 3489. Hoffmann, R. *J. Chem. Phys.* **1963**, *39*, 1397.

(44) Ammeter, J. H.; Burgi, H.-B.; Thibeault, J. C.; Hoffmann, R. *J. Am. Chem. Soc.* **1978**, *100*, 3686.

(45) Hoffman, D. M.; Hoffmann, R.; Fisel, C. R. *J. Am. Chem. Soc.* **1982**, *104*, 3858.

(46) Fujimoto, H.; Hoffmann, R. *J. Phys. Chem.* **1974**, *78*, 1167. Hoffmann, R.; Swenson, J. R.; Wan, C.-C. *J. Am. Chem. Soc.* **1973**, *95*, 7644.

A Simple High Energy Conformer Trapping Technique. Axial Phenylcyclohexane, NMR Spectra, and Thermodynamics

Michael E. Squillacote* and Joann M. Neth

Contribution from the Department of Chemistry, Brown University, Providence, Rhode Island 02912. Received January 3, 1986

Abstract: The axial conformer of phenylcyclohexane has been observed for the first time by using a unique but simple high-temperature cryogenic trapping technique. Thermodynamic and NMR spectral data have been obtained for this high-energy conformer, which is shown to have a perpendicular geometry. The NMR chemical shift differences between the equatorial and axial conformers are discussed in terms of their geometries and recent chemical shift theories.

Hassel first convincingly showed the existence of the two different positions of substitution on the chair form of a cyclohexane molecule.¹ He also recognized the preference of the equatorial position by any large group. However, the pioneering paper by Barton,² which pointed out the difference in chemical reactivity of these axial and equatorial substituents, catapulted these two conformers into the limelight of the chemical world. In fact, this discovery formed the cornerstone of the field of conformational analysis.³ Since that time, the axial-equatorial conformational energy difference and the spectroscopic differences (especially NMR shifts) of the two conformers of a variety of functionalities have been of great interest to chemists.⁴

One of the most interesting substituents on a cyclohexane molecule is a phenyl ring. This group has generated discussion for a number of reasons. Axially disposed phenyl groups are known to exist in a number of natural products.⁵ A phenyl substituent can adopt at least two different geometries in both the axial and equatorial positions.⁶ The phenyl group is a simple

substituent so knowledge of the NMR shift differences between the axial and equatorial conformers should offer insight into the controversy surrounding the origin of conformationally induced ¹³C chemical shifts.⁷⁻⁹ Finally, the phenyl group has been proposed as a ring locking group in preference to the *tert*-butyl since the latter has been shown to substantially distort the cyclohexane ring.¹⁰ These reasons combine to make the phenyl group an important reference point in the cyclohexane system.

Unfortunately, studies on the phenyl substituent have been hampered by the large free energy difference between the axial and equatorial conformer (the *A* value). Though several estimates for this free energy have been made,¹¹⁻¹³ the methods chosen for these studies have necessarily been indirect. Molecules selected for these experiments contain substituents in addition to the

(6) (a) Allinger, N. L.; Tribble, M. T. *Tetrahedron Lett.* **1971**, *35*, 3259-3262. (b) Eliel, E. L. *J. Mol. Struct.* **1985**, *126*, 385-400.

(7) Bierbeck, H.; Saunders, J. K. *Can. J. Chem.* **1976**, *54*, 2985-2995.

(8) Gorenstein, D. G. *J. Am. Chem. Soc.* **1977**, *99*, 2254-2258.

(9) (a) Lambert, J. B.; Vagenas, A. R. *Org. Magn. Reson.* **1981**, *17*, 270-277. (b) Lambert, J. B.; Vagenas, A. R. *Org. Magn. Reson.* **1981**, *17*, 265-269.

(10) Abraham, R. J.; Bergen, H. A.; Chadwick, D. J. *Tetrahedron Lett.* **1981**, *29*, 2807-2810.

(11) Garbisch, E. W.; Patterson, D. B. *J. Am. Chem. Soc.* **1963**, *85*, 3228-3231.

(12) Allinger, N. L.; Allinger, J.; DaRooge, M. A.; Greenberg, S. *J. Org. Chem.* **1962**, *27*, 4603-4606.

(13) Eliel, E. L.; Manoharan, M. *J. Org. Chem.* **1981**, *46*, 1959-1962.

(1) Hassel, O. *Tidsskr. Kjem. Berguesen Met.* **1943**, *3*, 32.

(2) Barton, D. H. R. *Experientia* **1950**, *6*, 316.

(3) Eliel, E. L. *J. Chem. Ed.* **1975**, *52*, 762.

(4) Hirsch, J. S. *Topics in Stereochemistry* **1967**, *1*, 199.

(5) (a) Jeffs, P. W.; Hawks, R. L.; Farrier, D. S. *J. Am. Chem. Soc.* **1969**, *91*, 3831-3839. (b) Capps, T. M.; Hargrave, K. D.; Jeffs, P. W.; McPhail, A. T. *J. Chem. Soc., Perkin Trans. 2* **1977**, 1098-1104. (c) Danishefsky, S.; Morris, J.; Mullen, G.; Gammill, R. *J. Am. Chem. Soc.* **1980**, *102*, 2838-2840.